

Response of high-altitude clouds to the galactic cosmic ray cycles around tropical regions

Hiroko Miyahara¹, Kanya Kusano², Ryuhō Kataoka³, and Emile Toubert⁴

¹Musashino Art University

²Nagoya University

³National Institute of Polar Research

⁴Okinawa Institute of Science and Technology

November 23, 2022

Abstract

Galactic cosmic rays (GCRs) are among the possible mediators of the solar influence on climate and weather. However, the impacts of GCR-induced ions on cloud formation and climate systems are not fully understood. In this paper, we show that the high-altitude clouds around the tropical regions associated with deep convective activities are susceptible to the decadal cycle of GCRs and that their impact and responding areas are seasonally variable. The most notable responses were found in August over land areas, suggesting that the susceptibility of clouds to GCRs may be dependent on the depth of convective activities and the abundance of aerosol precursor materials. We suggest that the positive feedback mechanism may be strengthening the GCR–cloud connection, maximizing the impact of GCR cycles with a lag of 1 year.

Hosted file

essoar.10511359.1.docx available at <https://authorea.com/users/546726/articles/602518-response-of-high-altitude-clouds-to-the-galactic-cosmic-ray-cycles-around-tropical-regions>

Response of high-altitude clouds to the galactic cosmic ray cycles around tropical regions

Hiroko Miyahara^{a,b,*}, Kanya Kusano^c, Ryuho Kataoka^{b,d,e}, and Emile Touber^{b,f}

^aHumanities and Sciences/Museum Careers, Musashino Art University, Tokyo 187-8505, Japan.

^bOkinawa Institute of Science and Technology, Okinawa 904-0495, Japan.

^cInstitute for Space-Earth Environmental Research, Nagoya University, Aichi 464-8601, Japan.

^dNational Institute of Polar Research, Tachikawa 190-8518, Japan.

^eSOKENDAI, The Graduate University for Advanced Studies, Kanagawa 240-0193, Japan.

^fDepartment of Mechanical Engineering, Imperial College London, London SW7 1AY, England

*Corresponding author: Hiroko Miyahara

Email: miyahara@musabi.ac.jp

Keywords: cosmic rays, clouds, Sun–Climate connection

Abstract

Galactic cosmic rays (GCRs) are among the possible mediators of the solar influence on climate and weather. However, the impacts of GCR-induced ions on cloud formation and climate systems are not fully understood. In this paper, we show that the high-altitude clouds around the tropical regions associated with deep convective activities are susceptible to the decadal cycle of GCRs and that their impact and responding areas are seasonally variable. The most notable responses were found in August over land areas, suggesting that the susceptibility of clouds to GCRs may be dependent on the depth of convective activities and the abundance of aerosol precursor materials. We suggest that the positive feedback mechanism may be strengthening the GCR–cloud connection, maximizing the impact of GCR cycles with a lag of 1 year.

Introduction

The possible responses of climate to variations in solar activity have been reported for a variety of time scales based on direct and proxy-based observations (Gray et al., 2010), and several mediating mechanisms have been proposed, including the effect of solar radiations (Kodera and Kuroda, 2002; Matthes et al., 2006; Meehl, 2008; Misios et al., 2019) and the influence of GCRs modulated by the solar wind magnetic field (Svensmark and Friis-Christensen, 1997; Carslaw et al., 2002).

Notable responses of climate to solar activity have been observed for millennial (Bond et al., 2001; Obrochta et al., 2012) and centennial time scales (Neff et al., 2001; Wang et al., 2005); however, identifying the relative importance of mediating solar-related parameters is difficult at such time scales, as the radiative and magnetic outputs of the Sun vary in complete correspondence. To identify the contribution of each of the parameters and trace the propagation of their impacts, it is needed to examine the shorter time scales, such as those associated with the solar decadal cycle, or even shorter, where the temporal variation of the solar radiative outputs and GCRs are slightly different (Miyahara et al., 2008; Yamaguchi et al., 2010).

Solar radiations vary based on the emergence and disappearance of sunspots and faculae and their migration on the solar surface (Domingo et al., 2009). Therefore, they change along with the decadal-scale variation of the activity level of sunspots. However, the flux of GCRs incident to the Earth's atmosphere is attenuated by the solar wind magnetic field in the heliosphere and is thus dependent on the evolution of the configuration and its direction (Jokipii and Thomas, 1981). As a result, shielding efficiency depends on the solar magnetic polarity that reverses every solar activity cycle maximum. The transient intensification of the magnetic fields associated with solar coronal mass ejections also enhances the shielding of GCRs (Forbush, 1938). Due to the travel time of the solar wind magnetic field in the heliosphere and its influence on the trajectory of GCRs, the variation of GCRs at Earth occasionally delay up to ~1.4 years relative to the decadal variations in solar activity level (Usoskin et al., 2001; Koldobskiy et al., 2022). Such features might allow identifying the potential contribution of GCRs to the decadal-scale Sun–Climate connection.

The possible impact of the decadal-scale solar activity on climate has been reported, for example, in the North Atlantic region (Kodera, 2002; Gray, 2016; Kuroda et al., 2022) and the tropical region (Gleisner and Thejll, 2003; van Loon et al., 2004; White, 2006; Misios et al., 2019). Recent studies have suggested that an increased solar activity results in a reduction in the east–west gradient of

the sea surface temperature (SST) over the Pacific Ocean and in a weakening of the Pacific Walker Circulation (Misios et al., 2019). These decadal-scale Sun–Climate connections have been mostly attempted to be explained by the so-called “top-down” mechanism, through which solar UV (SUV) influences stratospheric temperature and subsequently alters tropospheric circulation (Kodera and Kuroda, 2002; Matthes et al., 2006) or by the “bottom-up” mechanism, through which the total solar irradiance (TSI) warms up the ocean surface to change atmospheric circulation (Meehl, 2008; Misios et al., 2019). However, significant positive feedback is needed for the latter mechanism to explain the observed temperature variations, as the variability of TSI over solar cycles is as small as 1 W/m².

It is, however, also possible that GCRs contribute to the decadal-scale Sun–Climate connection through their impacts on clouds by the formation of cloud condensation nuclei (CCN) (Dickinson, 1975; Carslaw 2002; Kirkby et al., 2011; Svensmark et al., 2013), by enhancing the collision efficiency between aerosols and cloud droplets (Tinsley et al., 2000; Zhou et al., 2009), or by stabilizing the molecular cluster by the charges to grow to CCN (Tinsley and Deen, 1991; Yu and Turco, 2001; Yu, 2002). However, it is not well understood how their effects might proceed in actual environments and how those impacts might propagate in the climate system.

Originally, it was suggested that the cloud covers over oceans are enhanced with the increase in GCRs (Svensmark and Friis-Christensen, 1997). Later on, it was demonstrated that the low-altitude clouds over oceans are most significantly correlated to GCR variations (Marsh and Svensmark, 2003). However, both theoretical estimates and the laboratory chamber experiment simulating the GCR impact on CCN have indicated that cosmic-ray-induced CCN formations are rather efficient at low temperatures (i.e., at high altitudes) (Kazil, 2006; Yu et al., 2008; Kirkby et al., 2011). The upper troposphere is also favorable in terms of the abundance of cosmic-ray-induced ions (Ney, 1959; Ermakov et al., 1997; Usoskin et al., 2004).

It has been suggested that the impact of GCRs may only be emphasized if there are few preexisting aerosols in an ambient environment (Almeida et al., 2013), as newly formed aerosols tend to be adsorbed to preexisting aerosols if they are abundant. Atmospheric aerosols, including the ones that have anthropogenic origins, are mostly confined within ~4 km from the surface, except over the mountains with high elevations (Koffi et al., 2016). This factor also suggests that only the middle to upper troposphere may meet the criteria of significantly being impacted by GCRs. Deep convection is a possible method for supplying aerosol

precursors to CCN formations from the biogenic activities at the ground or ocean surfaces to the upper troposphere (Kazil 2006; Twohy et al., 2002); therefore, the high-altitude clouds near highly convective areas are potentially susceptible to the impact of GCRs.

In this paper, we examine this hypothesis by analyzing the variation of high-altitude clouds and its relation to GCR cycles, and discuss their possible impacts on the climate system. We used monthly-resolved high temporal-resolution cloud data to constrain the possible conditions required for clouds so as to significantly respond to GCR variations.

Results

Relationship between high-altitude clouds and GCR cycles

The monthly data of high-altitude clouds, as monitored by satellite observations, were compared with GCR cycles (see Methods). Then, it was found that there are regions in the tropics the high-altitude clouds show significant correlations to decadal-scale GCR cycles (Figure 1 and 2). However, the areas were localized, and they significantly varied based on the seasons (see Supplementary Figure S1–S12). Most significant correlations were found in August for the areas in which the formation of high-altitude clouds is active (see Figure 1e), supporting the above-mentioned hypothesis; however, they were localized to the land areas and proximate oceans. There were also some regions in which high cloud formations were suppressed (see below). In boreal winter, the areas showing significant correlations were migrated to the convective regions in the southern hemisphere (Figure 2). The signals were weaker compared with those of August; however, a relatively fast response was observed around the northern edge of Australia and the western limb of South America (Figure 2a).

The correlations were maximized in 1 year (Figure 1b and 2b) and were diminished afterward (Figure 1c–d and 2c–d). Such lagged responses imply that a positive feedback mechanism exists behind the GCR–cloud connection. The signals around the Indonesian Maritime Continent further delay, suggesting an impact through the mechanism involving atmospheric and ocean coupling. The maximal variability of the high-altitude cloud fraction over the largest GCR cycle since 1979 CE for a lag of 0–3 years is shown in Figures 1f and 2f. The maximal variability was found around India and was estimated to be ~25 %, which is a few tens of percent larger than the estimated variability of the ion production rates at the upper troposphere around the area (see Figure S12 of Dunne et al., 2016), also supporting the existence of a positive feedback mechanism.

Relationship between SST and the GCR cycles

Figure 3a–e indicates the correlation coefficient between SST and GCRs in August when the most notable correlations were found for cloud activity (for the relationships other than those of August, see Supplementary Figures S13–S23). The figures indicate that decadal-scale forcing results in a characteristic spatial pattern in the central and western Pacific. While the SST in the central Pacific tends to be cooled as GCR is enhanced, especially in the winter hemisphere, the SST in the southwestern Pacific tends to be warmed, suggesting that the trade winds over the Pacific region are intensified at the GCR cycle maxima. This tendency is consistent with the previously suggested reduced east–west SST gradient and the weaker trade winds at the solar cycle minima (Misios et al., 2019). However, the response of SST to TSI, which was suggested as the forcing parameter, delays by 1 year compared to the case of GCR and was maximized with a lag of 3 years (Figure 3k). The relationship between SST and SUV is more or less the same for TSI (see Supplementary Figure S24) and is peaked with a lag of ~3 years.

The areas showing significant correlations between SST and GCRs with no time lag were limited to the southern edge of the tropical zone around 20–30°S 100–130°W (Figure 3a); however, the impacts were expanded and maximized with a lag of 2 years (Figure 3c). The maximal temperature change over the largest GCR cycle since 1983 CE was as large as 1.7 K and was observed at the equator at around 160°E–160°W (Figure 3g). Regarding January, the east–west contrast was less well structured. However, the maximal change in the central Pacific reached 2.1 K (see Supplementary Figure S13).

Relationship between the surface pressure, zonal/meridional winds, and GCR cycles

The comparison between the surface pressure and GCRs (Figure 4a) indicates increased pressure around the southern edge of the tropical zone in the Pacific, and the impacts will be further intensified and expanded toward the northern hemisphere in 1–2 years (Figure 4b–c). On the contrary, the tropical regions between 120°W and 100°E indicate a tendency of decreasing pressure at the max GCR, especially over the oceans. The zonal and meridional wind speed compared with GCRs suggests a possible intensification of trade winds or a westerly migration of the deep convection core around the western Pacific, especially in the northern hemisphere (see Supplementary Figure S25). When the pressure data were compared with TSI, slightly different behaviors were recognized, other than the inversion of the response due to the anti-correlation of

GCR and TSI. One is the absence of immediate response, as in Figure 4g, and the other is the 1-year delay in the signals (Figure 4h–j) compared with the case for GCR (Figure 4a–c). The results for SUV are similar to those of TSI (Supplementary Figure S26), except for a possibly slightly faster response compared with the case of TSI.

Discussions

Although the decadal-scale impacts of solar activity have so far been mostly discussed under the framework of the above-mentioned “top-down” mechanism or “bottom-up” mechanism, the analyses of the cloud fractions and atmospheric and oceanic parameters suggest that another mechanism is possible: GCR’s impact on the atmospheric circulation and SST gradient through the activation of cloud formation.

The monthly-resolved high-resolution data allowed us to identify the areas where high-altitude clouds are susceptible to GCR variations and to understand the possible contributing factors determining their susceptibility, although high-resolution analyses might fail to capture the responses of the clouds that are propagated by winds and are not stationed. Significant positive correlations were found in tropical regions; however, they were limited to land and proximate oceans, suggesting the importance of any of or all the following factors: (1) the presence of relatively deeper convections compared with oceans, (2) the abundance of continental aerosol precursors for ions to produce CCN, and (3) a more pronounced diurnal cycle over lands (see below). Most of the notable correlations were found in August around West and Central Africa, India and Bangladesh, the northwestern coast of Southern America, and the nearby oceans, with a lag of 0–1 years (Figure 1a–b). The correlations in India and Bangladesh were concentrated between the Indian Ocean and the southern slopes of the Himalayan mountains, suggesting that the sea breezes blowing toward elevated mountains may also contribute to creating an environment in which cloud formations become sensitive to GCRs. The sea breezes blowing toward high mountains, similar to deep convection, uplifts a substantial amount of water vapor and aerosol precursors to the upper troposphere, where the ions produced by GCRs are most abundant. The signals around the western coast of South America in January (Figure 2a–c) and in the northwestern part of South America and southern Brazil in February (Figure S2a–c) may also be related to the same mechanism. Even though convective cloud formation is active over Brazil in January and February, the correlations were not significant except for the areas

facing oceans, thus suggesting the importance of marine aerosol precursors for the impact of ions.

The more pronounced impact in August, compared with January, can be associated with the seasonal variability in the emission of organic compounds from biogenic activities, the precursor materials for H₂SO₄ and amine, and thus for the CCN (Kirkby, 2007; Almeida et al., 2013). For example, the flux of dimethyl sulfide is maximum in the northern hemisphere from July to September and is especially enhanced around the northern part of the Indian Ocean (Land et al., 2014). The more significant impact in August might also be related to the relatively low pressure around the convective areas in August (Figure 4e, also see Figure S27), which provides ideal conditions for supplying water vapor and aerosol precursors to the upper troposphere. This low pressure also contributes to the higher GCR flux in the upper troposphere due to the reduced barometric effect (Mysowsky and Tuwim, 1926; Mendonça, 2013), although the associated enhancement is only a few percent.

Although the climatological condition is similar for July and August, the correlations between high-altitude clouds and GCRs are significantly different. The impact in July is sparse and not notable for a lag of 0-1 years except for around Central America (see Supplementary Figure S7a–b), while a significant increase was recognized around the Indonesian Maritime Continent for a lag of 2–3 years (see below). The possible explanation for the lack of a prompt response in July may be related to the influence of the updrafted preexisting aerosols masking the impact of GCRs (Almeida et al., 2013). For example, the abundance of mineral dust in northern Africa is maximum in June and starts to decrease in July (Vandenbussche et al., 2020). It has also been reported that the aerosol optical depth in northern India is maximum in May and that it starts to decrease in July (Gautam et al., 2010). Further examinations are, however, needed to confirm the impact of preexisting aerosols.

The tendency of the decreased pressure peaking with a lag of 1 year around tropical zones except for the Pacific region (Figure 4a–c) can be related to the activated formation of high-altitude clouds, and it may be causing positive feedback to the promotion of cloud formation. It has been suggested that the enhancement of aerosols may strengthen deep convection by freezing water droplets and releasing latent heat (Rosenfeld et al., 2008). The synchronized activation of convections over land in tropical regions may result in a tendency of decreased pressure around the area. The pressure decrease is more prominent over oceans and is significantly weaker over land, and this might be related to the more pronounced diurnal cycle over land (Yang and Slingo, 2001), which may

mask the signal of the transient pressure decrease in monthly mean data. However, the diurnal cycle over land may play an important role in sustaining convective activity as well as the supply of aerosol precursors to the upper troposphere even under enhanced cloud formation. In fact, the precipitation pattern indicates increased precipitation around the areas where high-altitude clouds are increased (see Supplementary Figure S28), supporting this tendency. Increased precipitation might also contribute to removing preexisting aerosols from the atmosphere.

The changed pressure gradient may then affect atmospheric circulation (Figure S25), allowing the change in the SST gradient over the Pacific Ocean (Figure 3a–e). The reduced formation of high-altitude clouds over the western Pacific (Figure 1a–b) can be explained by the westward relocation of deep convections around the area. Low-altitude clouds, instead, are likely increased around the western Pacific (Figure S29g–h). It is worth noting that this is a region of typhoon generation. While more high-altitude cloud activity is suggested for the higher GCR flux around the areas where hurricanes are generated, less typhoon activity is predicted for the higher GCR flux.

The westward extension of trade wind over the Pacific eventually warms the ocean around Indonesian Maritime Continent and off the northeast coast of Australia, and this warmth is maximized with a lag of 2–3 years (Figure 3c–d). The enhancement of high-altitude clouds around the area in July (see Figure S7) and August with a lag of 2–3 years can be related to this increased SST. The similar enhancement of high clouds with a lag of 2–3 years in October and November (Figures S10 and S11) should also be related to the increased SST.

The responses of SST and atmospheric circulation to the GCR cycles are similar to those suggested as a response to TSI cycles in previous studies; however, there are two notable differences. The first is the overall delay in the signals in the case compared with TSI (Figure 3h–l and Figure 4g–j), and the second is the warmth of the eastern Indian Ocean as an immediate response to TSI (Figure 3h). This feature, however, contradicts the weakening of the easterly wind in the western Pacific and the cooling tendency around the region suggested for the TSI maxima, as seen for the lag of 2–4 years (Figure 3j–l). Instead, it is more likely that this signal is related to the positive response to GCR with a lag of ~4 years (Figure 3e), which is a remnant of the impact around the Indonesian Maritime Continent (Figure 3d). In other words, a pseudo negative response with a five-year lag is expected for the case of TSI due to the delay of GCR to TSI by ~1 year. However, five years are nearly 180 degrees of a decadal solar cycle, thus resulting in the apparent immediate positive response to TSI (Figure 3h).

The possible solar influence pathway on climate systems through the variation of GCRs can be summarized as follows. First, GCRs impact the formation of high-altitude clouds around tropical regions, resulting in the decrease of pressure around the area, possibly giving positive feedback to cloud formation. Second, GCRs change atmospheric circulation and the SST pattern over the Pacific. Finally, altered SST patterns activate the high-altitude cloud formations around the Indonesian Maritime Continent. It is noteworthy that no correlation was observed around the eastern Pacific region, in which the interannual variation associated with the El Niño–Southern Oscillation (ENSO) is most prominent. It is, however, possible that the impact of GCRs contributes to the ENSO variability in the western Pacific, the occurrence of El Niño Modoki, the Indian Ocean Dipole, and possibly the Pacific Decadal Oscillation. The proposed impacts of GCRs on cloud activity and atmospheric circulation would shed light on the phase changes of such unresolved decadal-scale oceanic variations.

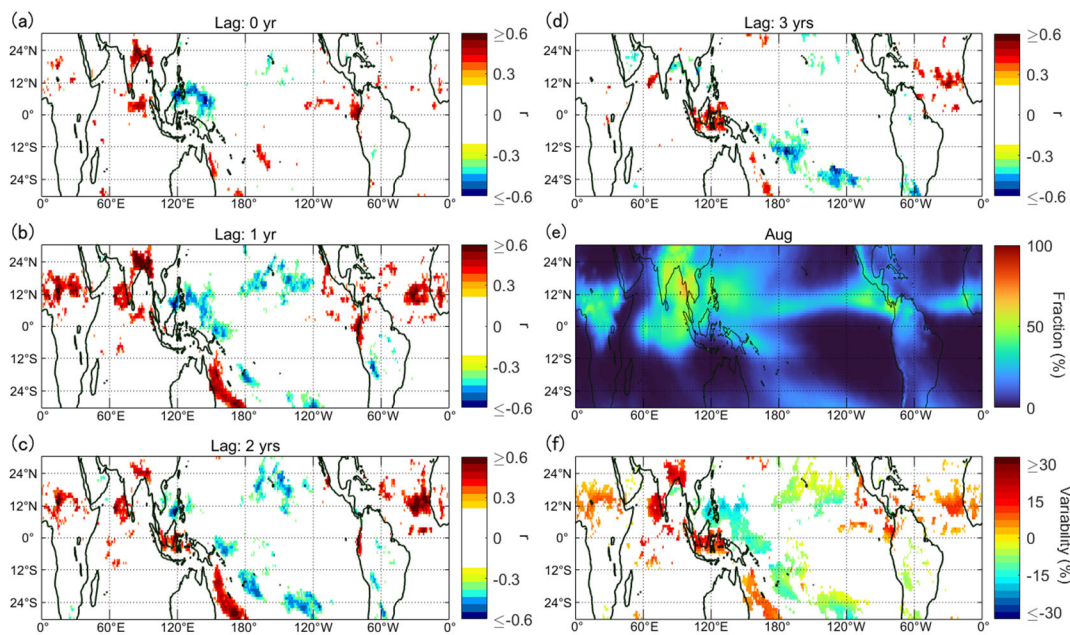


Figure 1. (a–d) Correlation coefficient r ($p \leq 0.05$) between GCRs and the high-altitude cloud fraction in August by ISCCP for a time lag of 0–3 years, respectively. (e) Monthly mean fraction of high-altitude clouds in August. (f) Maximal variability of the high-altitude cloud fraction over the GCR cycles.

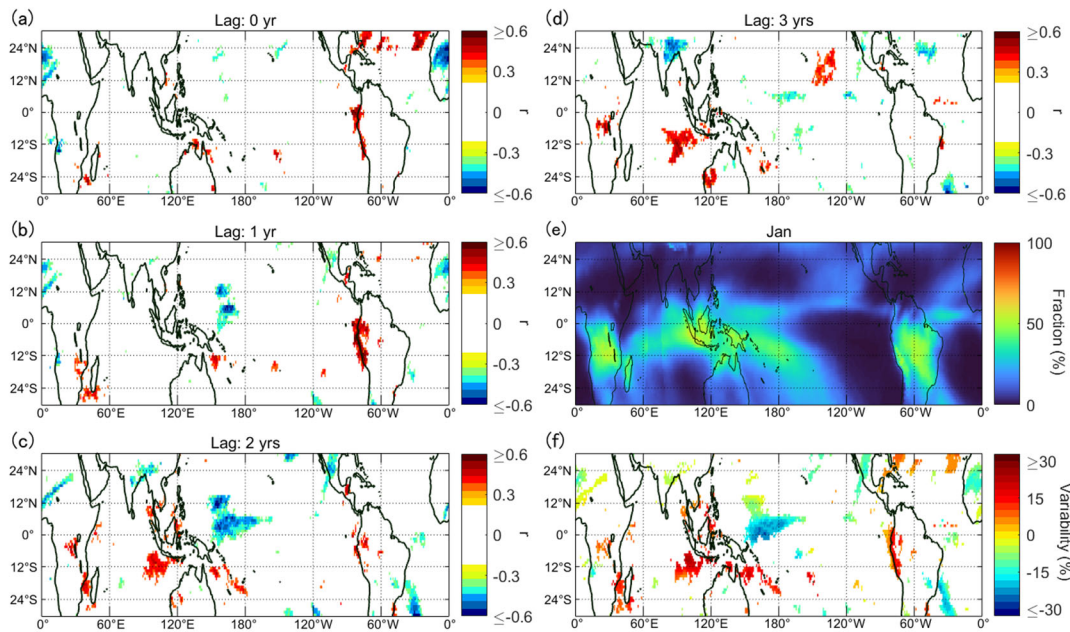


Figure 2. Same as Fig. 1 but for January.

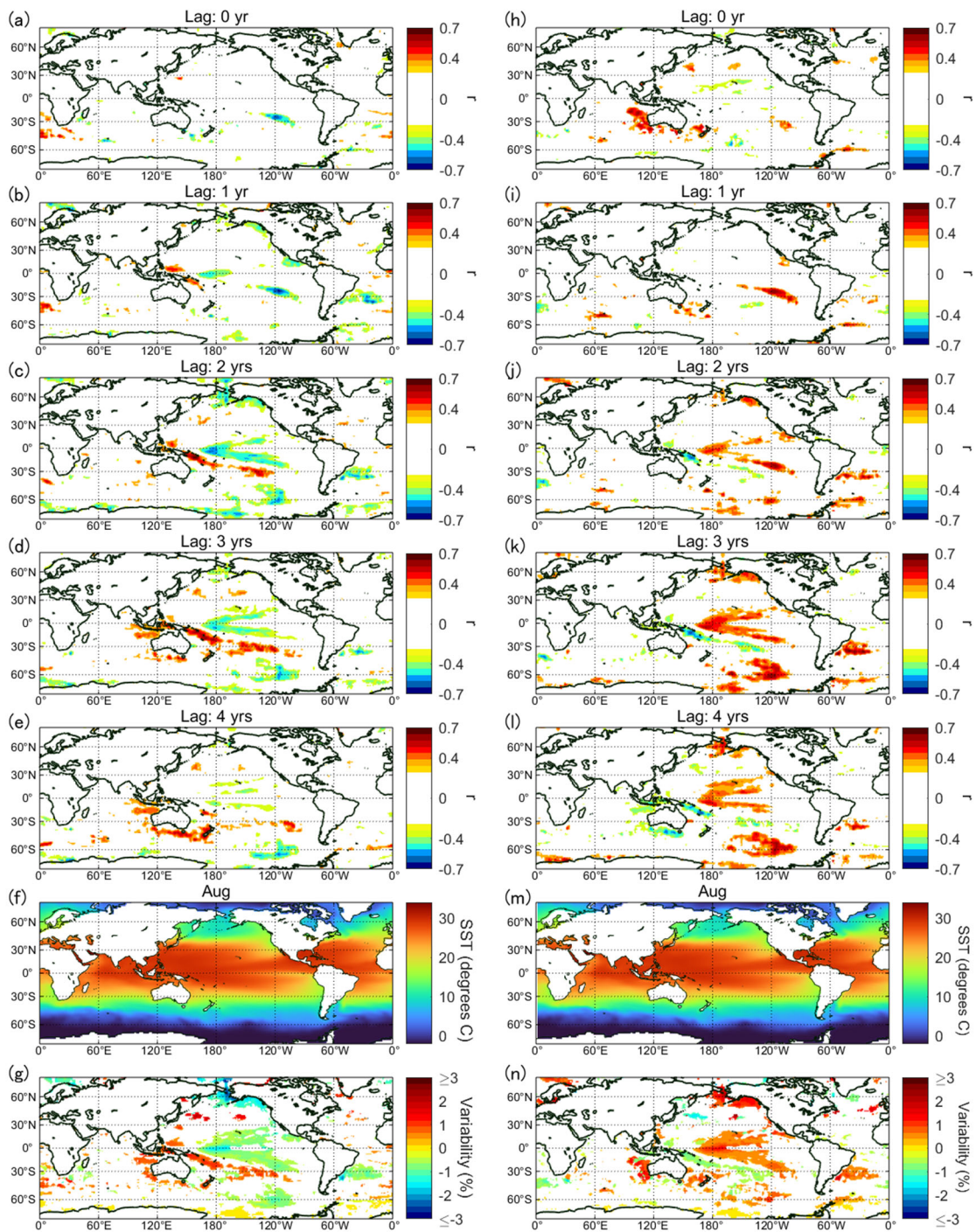


Figure 3. Comparison between SST and GCR/TSI. (a–e) Correlation coefficient r ($p \leq 0.05$) between GCRs and SST in August for a lag of 0–4 years, respectively. (f) Monthly mean SST for August. (g) Maximal variability of SST over the GCR cycles. (h–n) Same as (a–g) but for TSI.

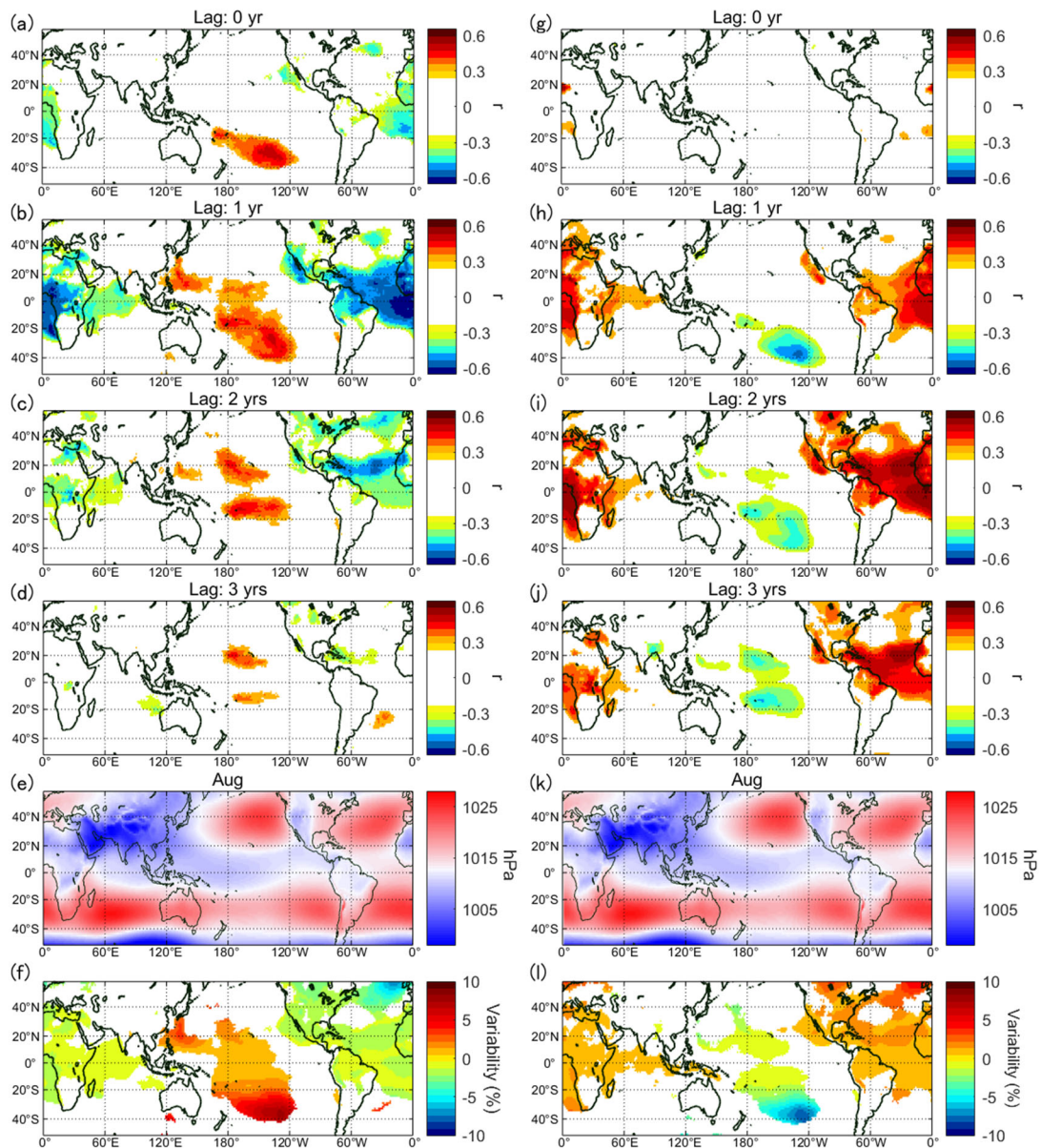


Figure 4. Comparison between the JRA-55 pressure reduced to the mean sea level and the GCRs/TSI variations. (a–d) Correlation coefficient r ($p \leq 0.05$) between pressure and GCRs in August for a lag of 0–3 years, respectively. (e) Monthly mean pressure reduced to the mean sea level for August. (f) Maximal variability of pressure over the GCR cycles. (g–l) Same as (a–f) but for TSI.

Methods

For this study, two cloud data sets were used to examine the possible response of high-altitude clouds to GCR decadal cycles. One is the ISCCP-H HGM series provided by the International Satellite Cloud Climatology Project (Rossow et al., 2016), and the other is the Outgoing Longwave Radiation (OLR) (Schreck et al., 2018). ISCCP-H HGM is the monthly mean product of cloud properties, including the fraction of high (≤ 440 mb), middle (440–680 mb), and low (>680 mb) clouds, covering the period of July/1983–June/2017. For this research, the monthly values of the high-altitude cloud fractions were used. We also utilized OLR data to validate the response of the ISCCP-H HGM data. We estimated the presence of high-altitude clouds by extracting daily data: ≤ 200 W/m² for each 1-degree grid. The fraction of the days was obtained for each month. It was confirmed that they show consistent variations with the ISCCP-H HGM high clouds for the low-latitude regions (30S–30N). The data were then compared with the GCR variation. In this study, we used the OLR data for Jan/1979–Dec/2021. For the GCR variation, the Climax neutron monitor data (<http://cr0.izmiran.ru/clmx/main.htm>) and Oulu neutron monitor data (<http://cr0.izmiran.ru/oulu/main.htm>) were used. The daily data were adjusted and averaged to obtain the monthly mean values. To examine the response of the high-altitude clouds to GCR and the possible feedbacks that may accompany some time lags, Spearman's correlation coefficient between the high-altitude clouds and GCRs were obtained for each 1-degree grid for the lag of 0–3 years. To estimate the correlation coefficient at a lag of zero years, the correlation coefficients for –2 years (GCRs lag cloud variation with 2 years) to 0 years (no time lag) were calculated, and only the case correlations maximized at 0 years were displayed in the map. For the zero-year lag, the cloud data were compared with the monthly mean GCR flux and with the yearly mean for a lag of 1 year or longer. For the grids where the high-altitude clouds were absent for more than fifty percent of the analyzed years, we excluded them from the analyses. For the area significant correlation with $p \leq 0.05$ was found, the maximal variability of high-altitude clouds over the GCR cycles was estimated, i.e., the variability for the largest GCR cycle since 1979 CE. Prior to the analyses, the long-term trends were subtracted from both the cloud and GCR data to concentrate on the decadal-scale variations.

For the examination of the response of SST to the GCR cycles, we used the NOAA_OI_SST_V2 data provided by NOAA/OAR/ESRL PSL, Boulder, Colorado, USA on their website: <https://psl.noaa.gov/data/gridded/data.noaa.oisst.v2.html>. We used the 1-degree grid data for the period of Dec/1981–Dec/2021. To analyze the surface pressure response to the GCR cycles, we used the 1-degree grid

reanalysis data of the JRA-55 monthly mean pressure reduced to mean sea level. We only used data from 1979 when the observational data was substantial and the reliability was high (Ebita et al., 2011). For the precipitation analysis, we used CMAP monthly mean precipitation data provided by NOAA/OAR/ESRL PSL, Boulder, Colorado, USA on their website: <https://psl.noaa.gov/data/gridded/data.cmap.html>.

To examine the responses of SST and atmospheric data to TSI, the NOAA Climate Data Record of TSI (Coddington et al., 2015) was used. As an index of solar UV, NOAA adjusted the solar radio flux at 10.7cm (https://lasp.colorado.edu/lisird/data/noaa_radio_flux/) were combined with the Penticton radio flux data for May/2018 to present (https://lasp.colorado.edu/lisird/data/penticton_radio_flux/).

Note that the data from Jun/1991 to May/1993 were excluded from the above analyses so that the possible impacts from the eruption of Mt. Pinatubo in 1991 are eliminated.

Acknowledgments

We thank S. Masuda, H. Yamada, Y. Yamashiki, K. Munakata, for discussions. This work was supported by JSPS KAKENHI grand number 15H05816 and the research scholarship provided to Musashino Art University by H. Suzuki. H.M. thanks Okinawa Institute of Science and Technology for hosting her sabbatical visit.

Reference

Gray, L. J., et al., Solar influences on climate, *Rev. Geophys.*, 48, RG4001, doi:[10.1029/2009RG000282](https://doi.org/10.1029/2009RG000282) (2010).

Kodera, K. & Kuroda, Y., Dynamical response to the solar cycle, *Journal of Geophysical Research* 107, 4749 (2002).

Matthes, K., Kuroda, Y., Kodera, K., and Langematz, U., Transfer of the solar signal from the stratosphere to the troposphere: Northern winter, *Journal of Geophysical Research* 111, D06108 (2006).

Meehl, G.A., Arblaster, J.M., Branstator, G., and van Loon, H., A coupled air–sea response mechanism to solar forcing in the Pacific region, *Journal of Climate* 21,

2883–2897 (2008).

Misios, S., et al., Slowdown of the Walker circulation at Solar Cycle Maximum, *Proceedings of the National Academy of Sciences of the United States of America* 116, 7186–7191 (2019).

Svensmark, H., and Friis-Christensen, E., Variation of cosmic ray flux and global cloud coverage—A missing link in solar-climate relationships, *Journal of Atmospheric and Solar-Terrestrial Physics* 59, 1225–1232, doi:[10.1016/S1364-6826\(97\)00001-1](https://doi.org/10.1016/S1364-6826(97)00001-1) (1997).

Carslaw, K.S., Harrison, R.G., and Kirkby, J., Cosmic rays, clouds, and climate, *Science* 298, 1732–1737 (2002).

Bond, G.C. et al., Persistent solar influence on North Atlantic climate during the Holocene, *Science* 294, 2130–2136 (2001).

Obrochta, S.P., Miyahara, H., Yokoyama, Y., and Crowley, T.J., A re-examination of evidence for the North Atlantic “1500-year cycle” at Site 609, *Quaternary Science Reviews* 55, 23–33 (2012).

Neff, U., et al., Strong coherence between solar variability and the monsoon in Oman between 9 and 6 kyr ago, *Nature* 411, 290–293 (2001).

Wang, Y., et al., The Holocene Asian monsoon: Links to solar changes and North Atlantic climate, *Science* 308, 854–857 (2005).

Miyahara, H., Yokoyama, Y., and Masuda, K., Possible link between multi-decadal climate cycles and periodic reversals of solar magnetic field polarity, *Earth and Planetary Science Letters* 272, 290–295 (2008).

Yamaguchi, Y.T., Yokoyama, Y., Miyahara, H., Sho, K., and Nakatsuka, T., Synchronized Northern Hemisphere climate change and solar magnetic cycles during the Maunder Minimum, *Proceedings of the National Academy of Sciences of the United States of America* 107, 20697–20702 (2010).

Domingo, V., et al., Solar surface magnetism and irradiance on time scales from days to the 11-year cycle, *Space Science Reviews* 145, 337–380 (2009).

Jokipii, J.R., and Thomas, B., Effects of drift on the transport of cosmic rays. IV. Modulation by a wavy interplanetary current sheet, *The Astrophysical Journal* 243, 1115–1122 (1981).

Forbush, S.E., On cosmic-ray effects associated with magnetic storms, *Journal of Geophysical Research* 43, 203–218, doi:[10.1029/TE043i003p00203](https://doi.org/10.1029/TE043i003p00203) (1938).

Usoskin, I.G., Mursula, K., Kananen, H., and Kovaltsov, G.A., Dependence of cosmic rays on solar activity for odd and even solar cycles, *Advances in Space Research* 27, 571–576 (2001).

Koldobskiy, S.A. et al., Time lag between cosmic-ray and solar variability: Sunspot Numbers numbers and open solar magnetic flux, *Solar Physics* 297, 38 (2022).

Kodera, K., Solar cycle modulation of the North Atlantic Oscillation: Implication in the spatial structure of the NAO, *Geophysical Research Letters* 29, 59–51, doi:[10.1029/2001GL014557](https://doi.org/10.1029/2001GL014557) (2002).

Gray, L.J., Woollings, T.J., Andrews, M., and Knight, J., Eleven-year solar cycle signal in the NAO and Atlantic/European blocking, *Quarterly Journal of the Royal Meteorological Society* 142, 1890–1903 (2016).

Kuroda, Y., Kodera, K., Yoshida, K., Yukimoto, S., and Gray, L., Influence of the solar cycle on the North Atlantic oscillation, *Journal of Geophysical Research: Atmospheres* 127, e2021 (2022).

Gleisner, H., and Thejll, P., Patterns of tropospheric response to solar variability, *Geophysical Research Letters* 30, 1711, doi:[10.1029/2003GL017129](https://doi.org/10.1029/2003GL017129) (2003).

van Loon, H., Meehl, G.A., and Arblaster, J.M., A decadal solar effect in the tropics in July–August, *Journal of Atmospheric and Solar-Terrestrial Physics* 66, 1767–1778 (2004).

White, W.B., Response of tropical global ocean temperature to the Sun's quasi-decadal UV radiative forcing of the stratosphere, *Journal of Geophysical Research* 111, C09020 (2006).

Dickinson, R.E., Solar variability and the lower atmosphere, *Bulletin of the American Meteorological Society* 56, 1240–1248 (1975).

Kirkby, J. et al., Role of sulphuric acid, ammonia and galactic cosmic rays in atmospheric aerosol nucleation, *Nature* 476, 429–433 (2011).

Svensmark, H., Enghoff, M.B., and Pedersen, J.O.P., Response of cloud condensation nuclei (> 50 nm) to changes in ion-nucleation, *Physics Letters A* 377, 2343–2347 (2013).

Tinsley, B.A., Influence of solar wind on the global electric circuit, and inferred effects on cloud microphysics, temperature, and dynamics in the troposphere, *Space Science Reviews* 94, 231–258 (2000).

Zhou, L., Tinsley, B.A., and Plemmons, A., Scavenging in weakly electrified saturated and subsaturated clouds, treating aerosol particles and droplets as conducting spheres, *Journal of Geophysical Research* 114, D18201, doi:[10.1029/2008JD011527](https://doi.org/10.1029/2008JD011527) (2009).

Tinsley, B.A., and Deen, G.W., Apparent tropospheric response to MeV-GeV particle flux variations: A connection via electrofreezing of supercooled water in high-level clouds?, *Journal of Geophysical Research* 96, 22283–22296, doi:[10.1029/91JD02473](https://doi.org/10.1029/91JD02473) (1991).

Yu, F., and Turco, R.P., From molecular clusters to nanoparticles: Role of ambient ionization in tropospheric aerosol formation, *Journal of Geophysical Research: Atmospheres* 106, 4797–4814 (2001).

Yu, F., Altitude variations of cosmic ray induced production of aerosols: Implications for global cloudiness and climate, *Journal of Geophysical Research* 107, A7 (2002).

Marsh, N., and Svensmark, H., Galactic cosmic ray and el Niño–Southern Oscillation trends in International Satellite Cloud Climatology Project D2 low-cloud properties, *Journal of Geophysical Research: Atmospheres* 108, 4195, doi:[10.1029/2001JD001264](https://doi.org/10.1029/2001JD001264) (2003).

Kazil, J., Lovejoy, E.R., Barth, M.C., and O'Brien, K., Aerosol nucleation over oceans and the role of galactic cosmic rays, *Atmospheric Chemistry and Physics* 6, 4905–4924 (2006).

Yu, F., Wang, Z., Luo, G., and Turco, R., Ion-mediated nucleation as an important global source of tropospheric aerosols, *Atmospheric Chemistry and Physics* 8, 2537–2554 (2008).

Ney, E.R., Cosmic radiation and weather, *Nature* 183, 451–452 (1959).

Ermakov, V.I., Bazilevskaya, G.A., Pokrevsky, P.E., and Stozhkov, Y.I., Ion balance equation in the atmosphere, *Journal of Geophysical Research: Atmospheres* 102, 23413–23419 (1997).

Usoskin, I.G., Gladysheva, O.G., and Kovaltsov, G.A., Cosmic ray-induced ionization in the atmosphere: Spatial and temporal changes, *Journal of Atmospheric and Solar-Terrestrial Physics* 66, 1791–1796 (2004).

Almeida, J., et al., Molecular understanding of sulphuric acid–amine particle nucleation in the atmosphere, *Nature* 502, 359–363 (2013).

Koffi, B., et al., Evaluation of the aerosol vertical distribution in global aerosol models through comparison against CALIOP measurements: AeroCom phase II results, *Journal of Geophysical Research: Atmospheres* 121, 7254–7283 (2016).

Twohy, C.H., et al., Deep convection as a source of new particles in the midlatitude upper troposphere, *Journal of Geophysical Research: Atmospheres* 107, AAC 6–AAC 1, doi:[10.1029/2001JD000323](https://doi.org/10.1029/2001JD000323) (2002).

Dunne, E.M., et al., Global atmospheric particle formation from CERN CLOUD measurements, *Science* 354, 1119–1124 (2016).

Kirkby, J., Cosmic rays and climate, *Surveys in Geophysics* 28, 333–375 (2007).

Land, P.E., Shutler, J.D., Bell, T.G., and Yang, M., Exploiting satellite Earth observation to quantify current global oceanic DMS flux and its future climate sensitivity, *Journal of Geophysical Research: Oceans* 119, 7725–7740, doi:[10.1002/2014JC010104](https://doi.org/10.1002/2014JC010104) (2014).

Myssowsky, L., and Tuwim, L., Unregelmässige Intensitätsschwankungen der Hohenstrahlung in geringer Seehöhe, Zeitschrift für Physik A – Hadrons and Nuclei 39, 146–150, doi:[10.1007/BF01394307](https://doi.org/10.1007/BF01394307) (1926).

De Mendonça, R.R.S., Raulin, J.-P., Echer, E., Makhmutov, V.S., and Fernandez, G., Analysis of atmospheric pressure and temperature effects on cosmic ray measurements, Journal of Geophysical Research: Space Physics 118, 1403–1409, doi:[10.1029/2012JA018026](https://doi.org/10.1029/2012JA018026) (2013).

Vandenbussche, S., Callewaert, S., Schepanski, K., and De Mazière, M., North African mineral dust sources: New insights from a combined analysis based on 3D dust aerosol distributions, surface winds and ancillary soil parameters, Atmospheric Chemistry and Physics 20, 15127–15146 (2020).

Gautam, R., Hsu, N.C., and Lau, K.-M., Premonsoon aerosol characterization and radiative effects over the Indo-Gangetic Plains: Implications for regional climate warming, Journal of Geophysical Research 115, D17208, doi:[10.1029/2010JD013819](https://doi.org/10.1029/2010JD013819) (2010).

Rosenfeld, D., et al., Flood or drought: How do aerosols affect precipitation?, Science 321, 1309–1313 (2008).

Yang, G.-Y., and Slingo, J., The diurnal cycle in the tropics, Monthly Weather Review 129, 784–801 (2001).

Rosow, W.B. et al.; and NOAA's Climate Data Record Program (2016), International Satellite Cloud Climatology Project Climate Data Record, H-Series HGM NOAA National Centers for Environmental Information, doi:[10.7289/V5QZ281S](https://doi.org/10.7289/V5QZ281S).

Schreck, C.J., Lee, H.-T., and Knapp, K.R., HIRS outgoing longwave radiation—Daily climate data record: Application toward identifying tropical subseasonal variability, Remote Sensing 10, 1325, doi:[10.3390/rs10091325](https://doi.org/10.3390/rs10091325) (2018).

Ebita, A., et al., The Japanese 55-year Reanalysis “JRA-55”: An Interim Report, Sola 7, 149–152 (2011).

Coddington, O., et al., NOAA Climate Data Record (CDR) of Total Solar Irradiance (TSI), NRLTSI version 2, N.O.A.A. National Centers for Environmental Information, doi:[10.7289/V55B00C1](https://doi.org/10.7289/V55B00C1) (2015).

Author contributions

H.M. designed the study with input from K.K. H.M. performed data analyses and wrote the manuscript with input from all of the other authors.

Competing interests

Authors declare no competing interests.

Additional information

Supplementary Information are available for this paper.

Supplementary materials

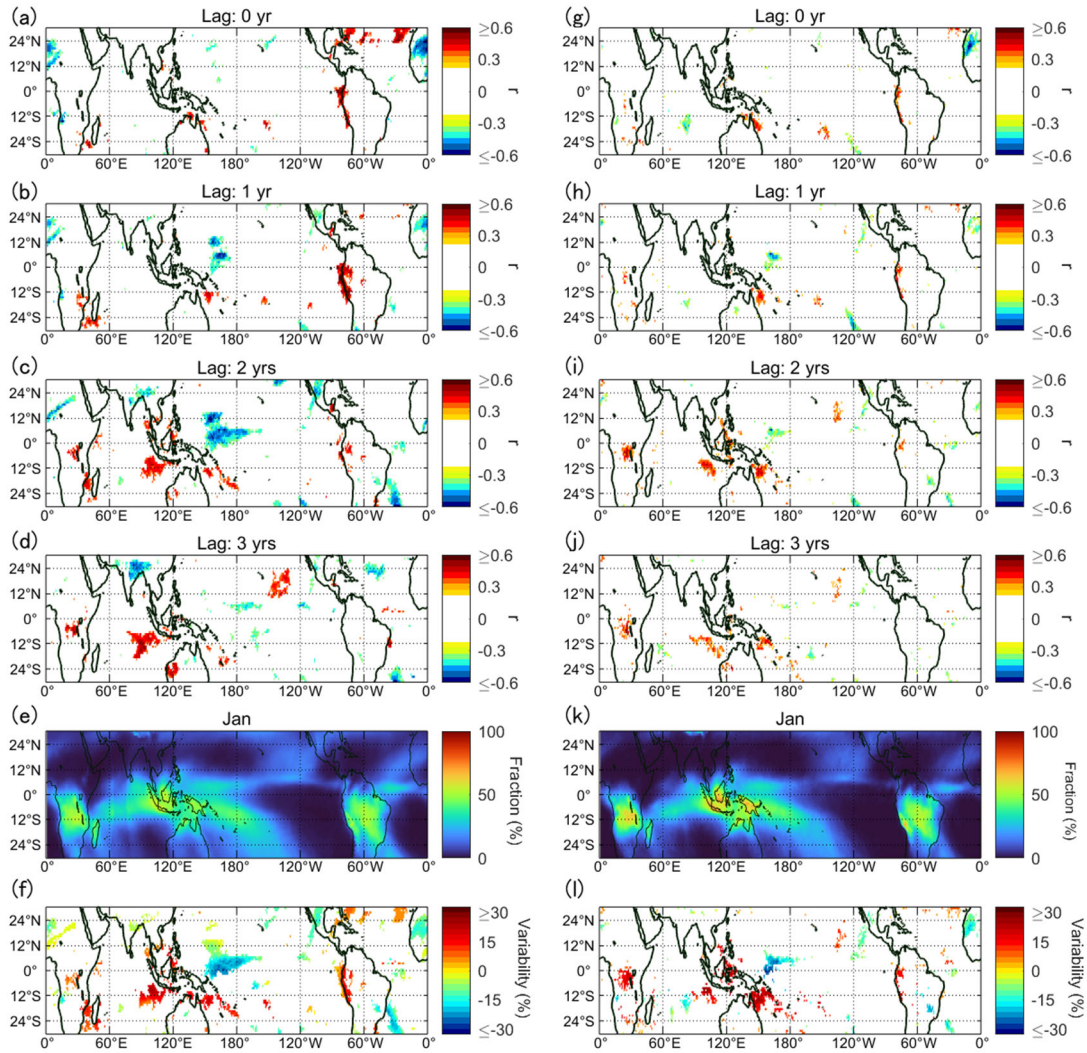


Figure S1. (a-d) Correlation coefficient r ($p \leq 0.05$) between GCRs and the high-altitude cloud fraction in January by ISCCP for a time lag of 0–3years, respectively. (e) Monthly mean fraction of the high-altitude clouds in January. (f) Maximal variability of the high-altitude cloud fraction over the GCR cycles. (g-l) Same as (a-f) but for the high-altitude clouds, as monitored using OLR.

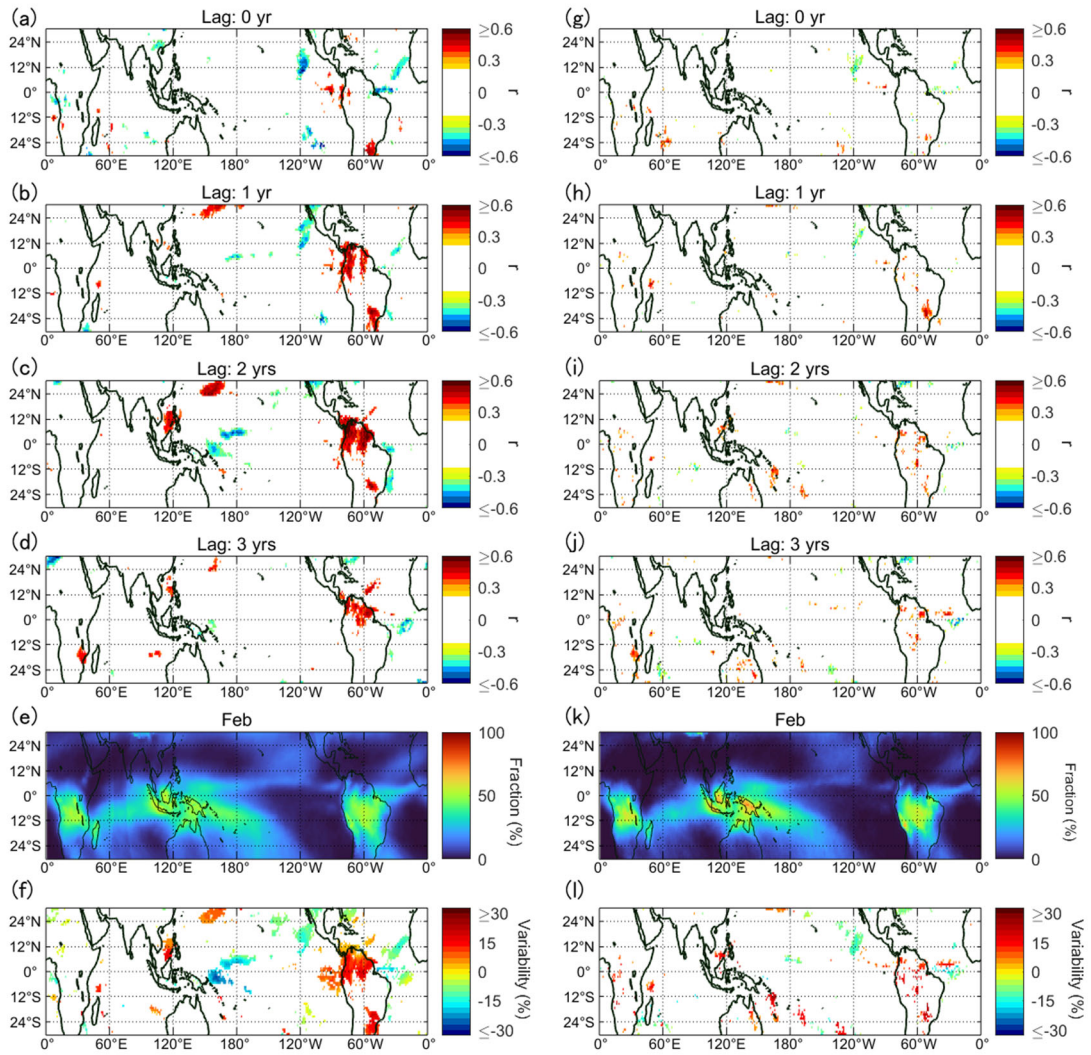


Figure S2. Same as Fig. S1 but for February.

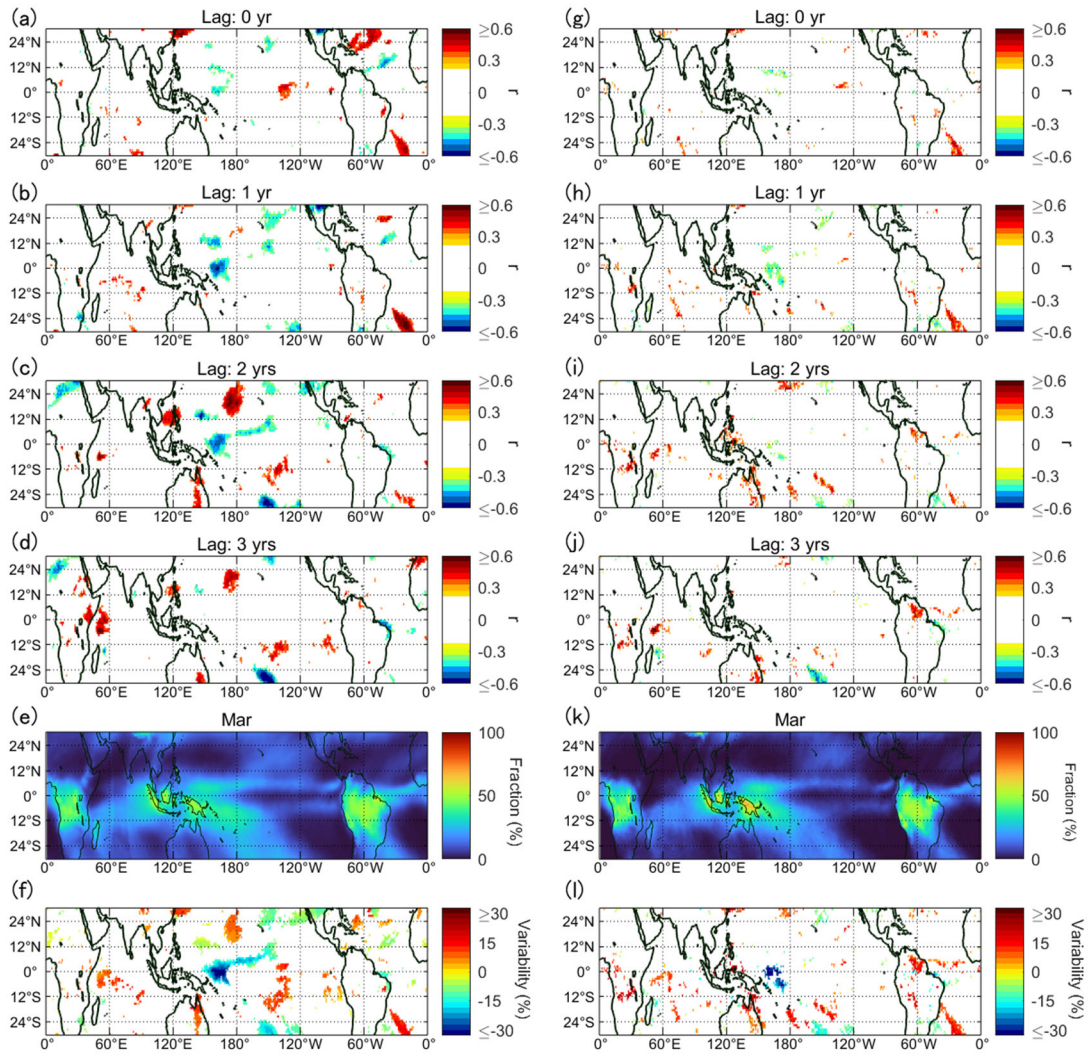


Figure S3. Same as Fig. S1 but for March.

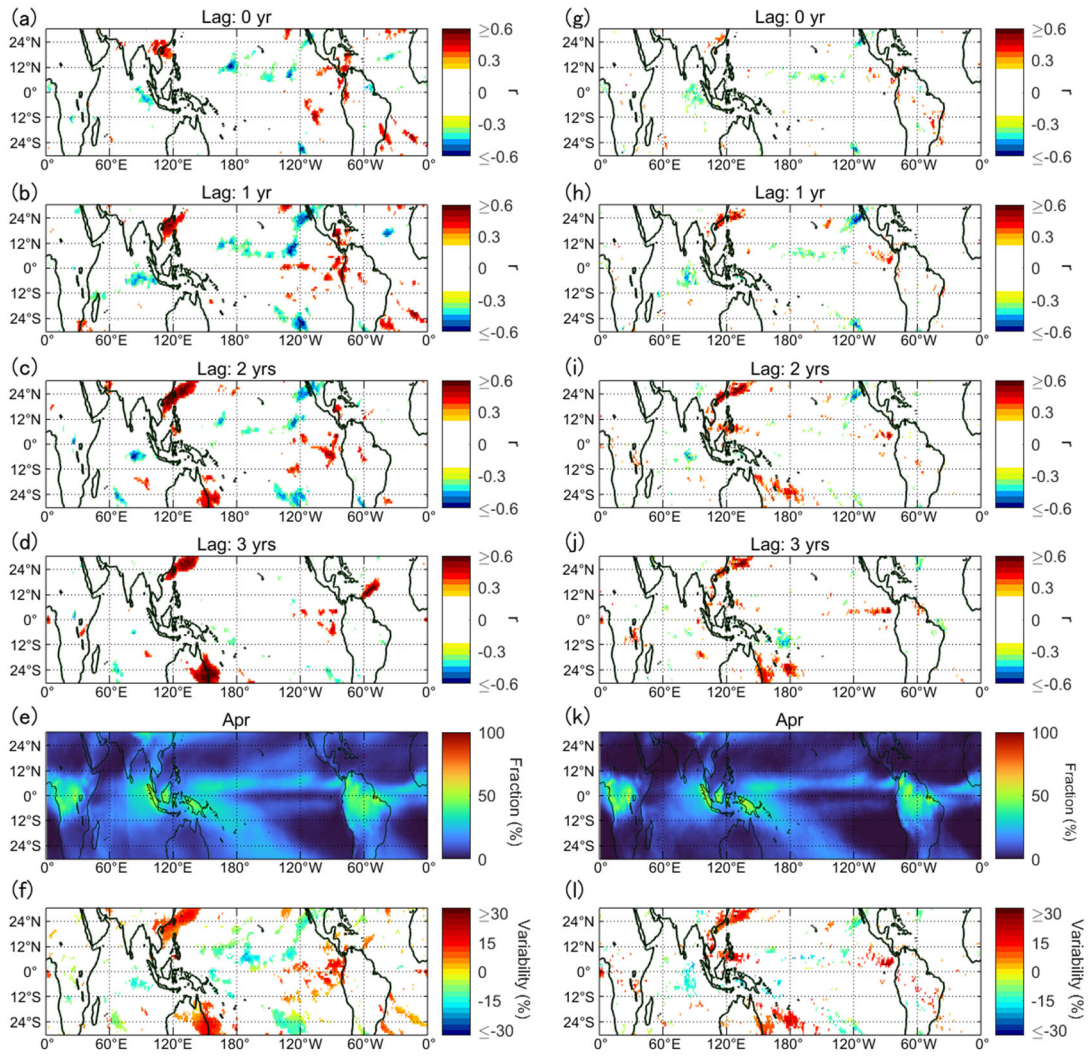


Figure S4. Same as Fig. S1 but for April.

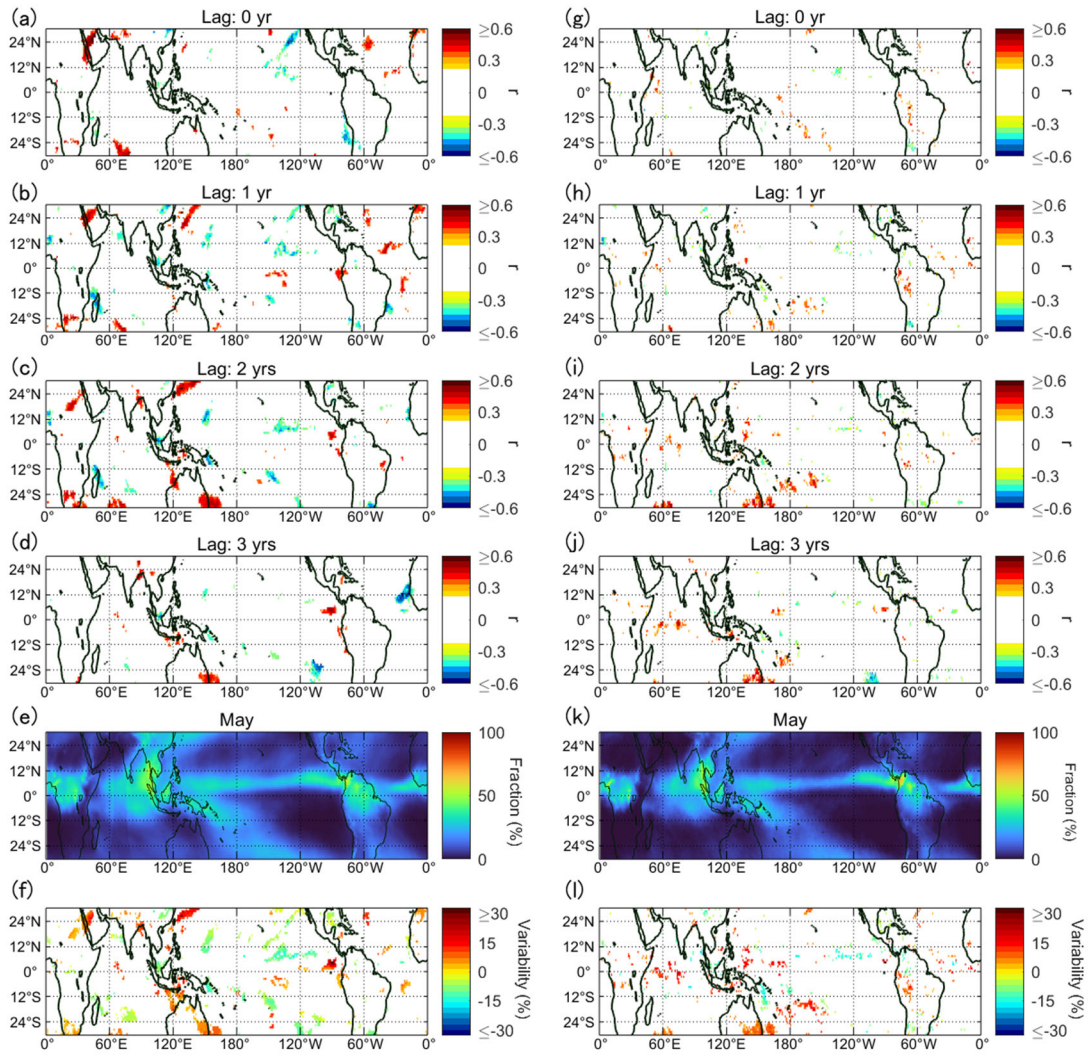


Figure S5. Same as Fig. S1 but for May.

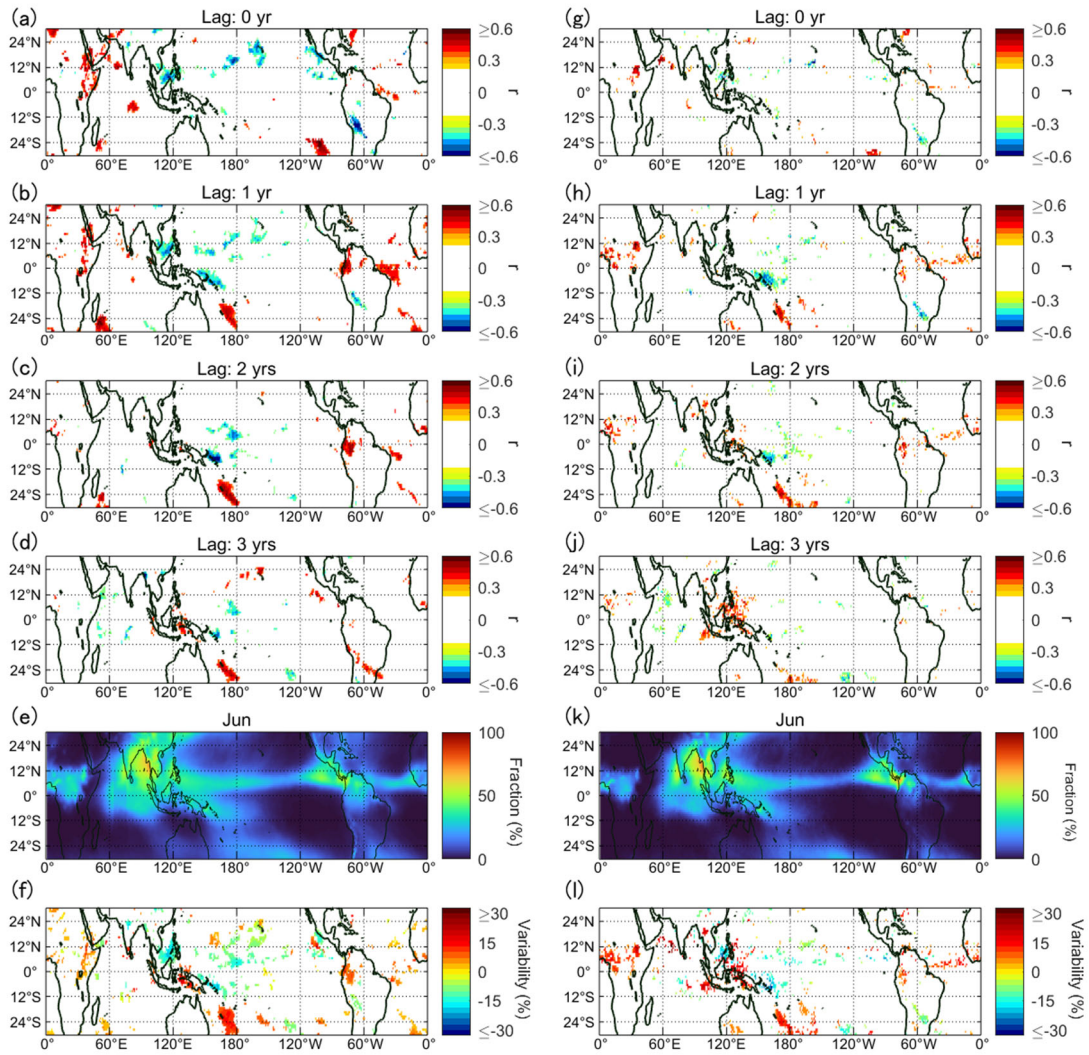


Figure S6. Same as Fig. S1 but for June.

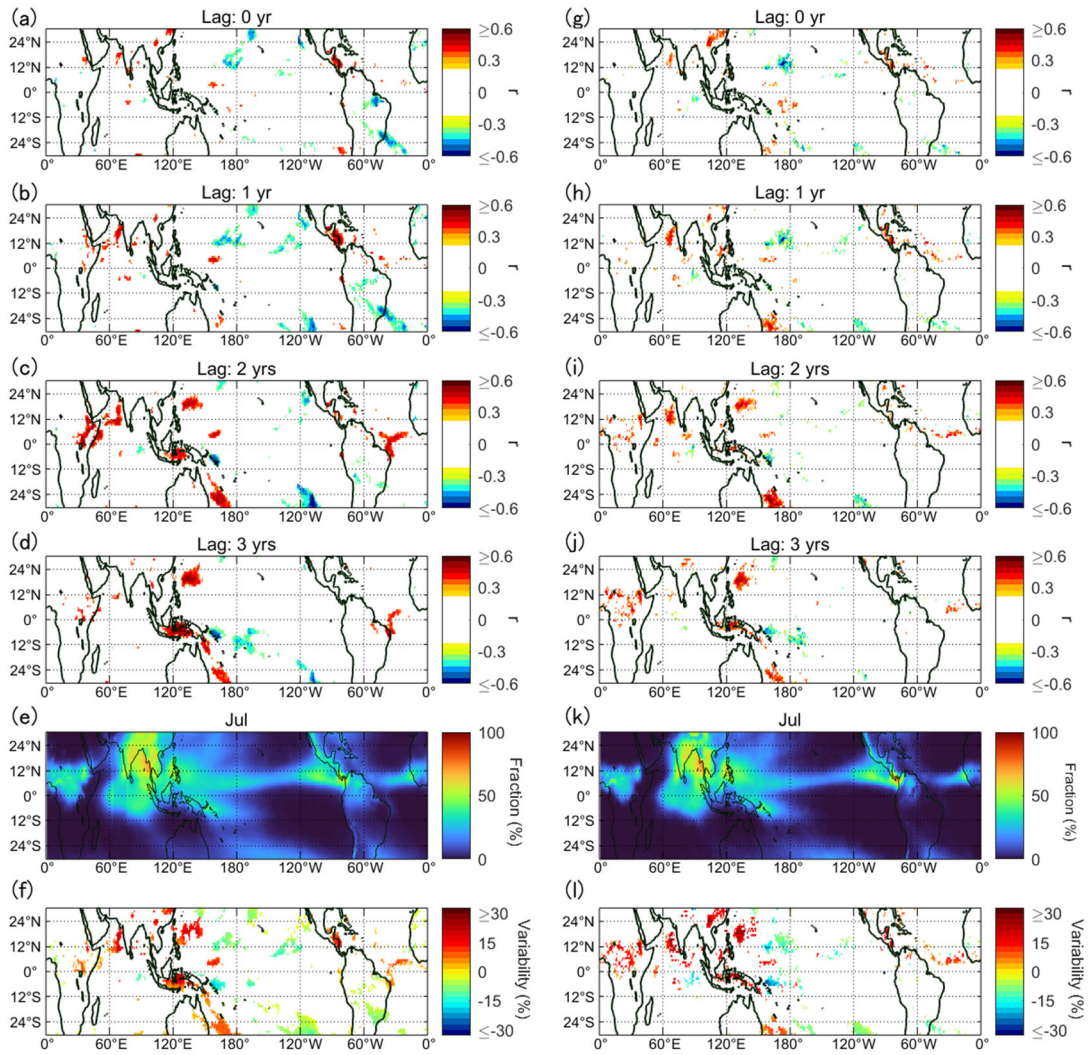


Figure S7. Same as Fig. S1 but for July.

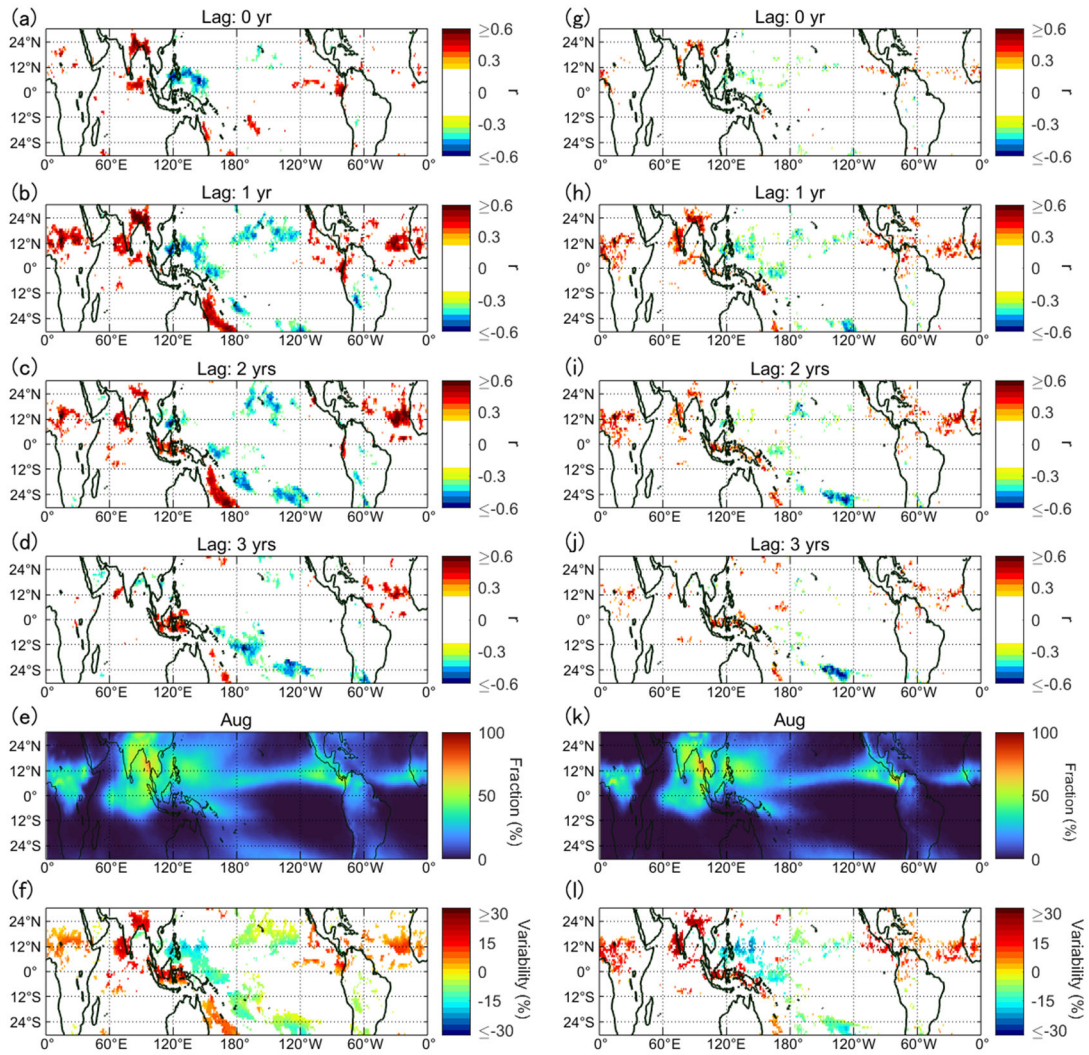


Figure S8. Same as Fig. S1 but for August.

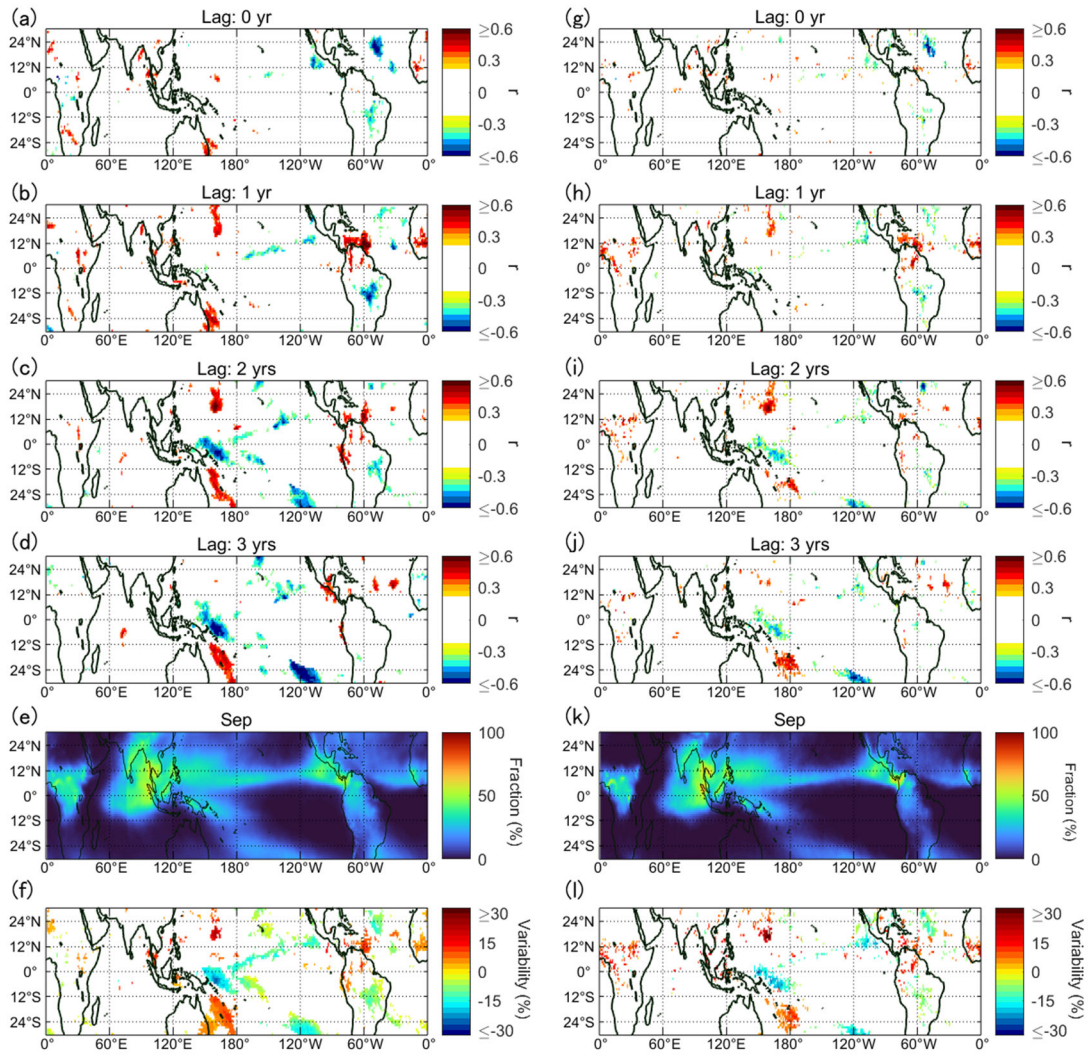


Figure S9. Same as Fig. S1 but for September.

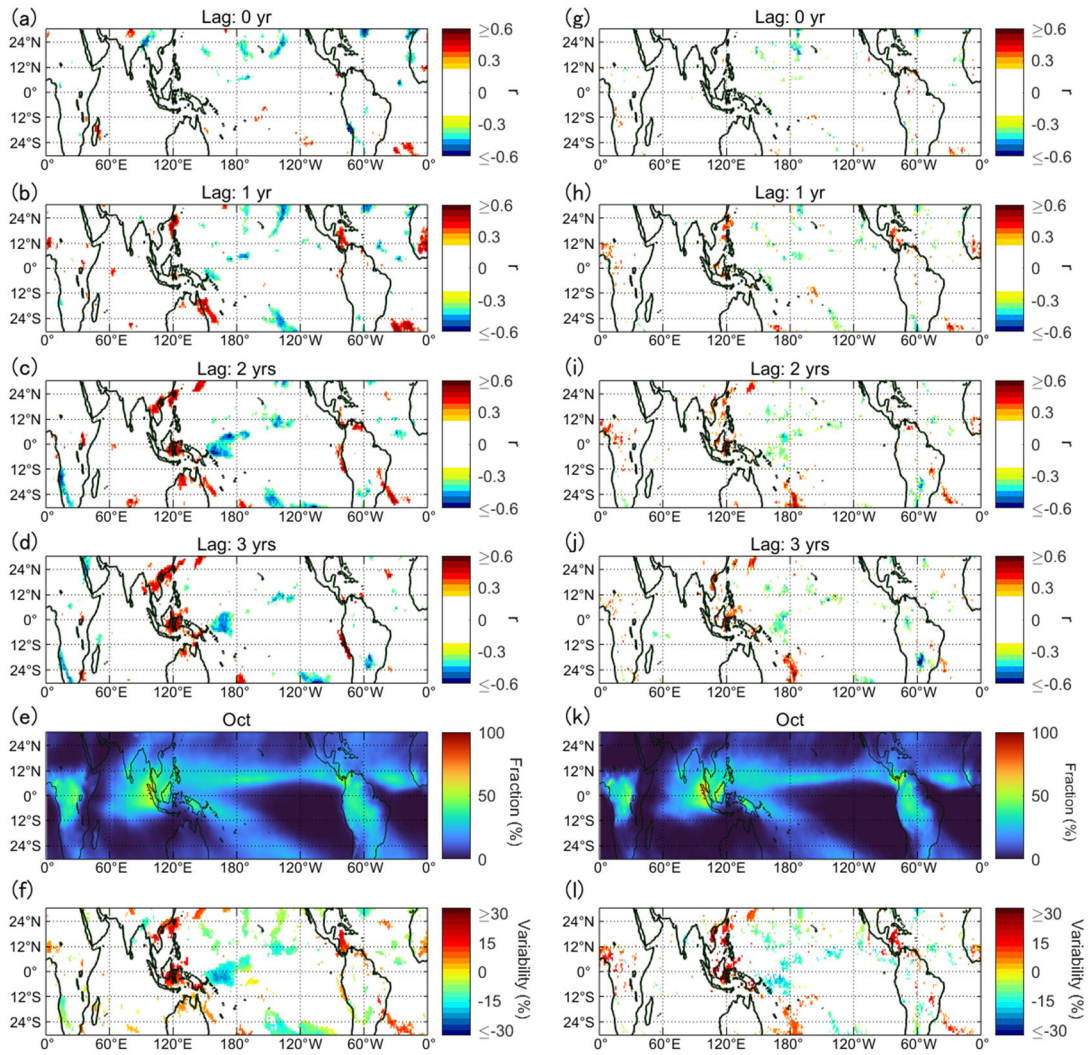


Figure S10. Same as Fig. S1 but for October.

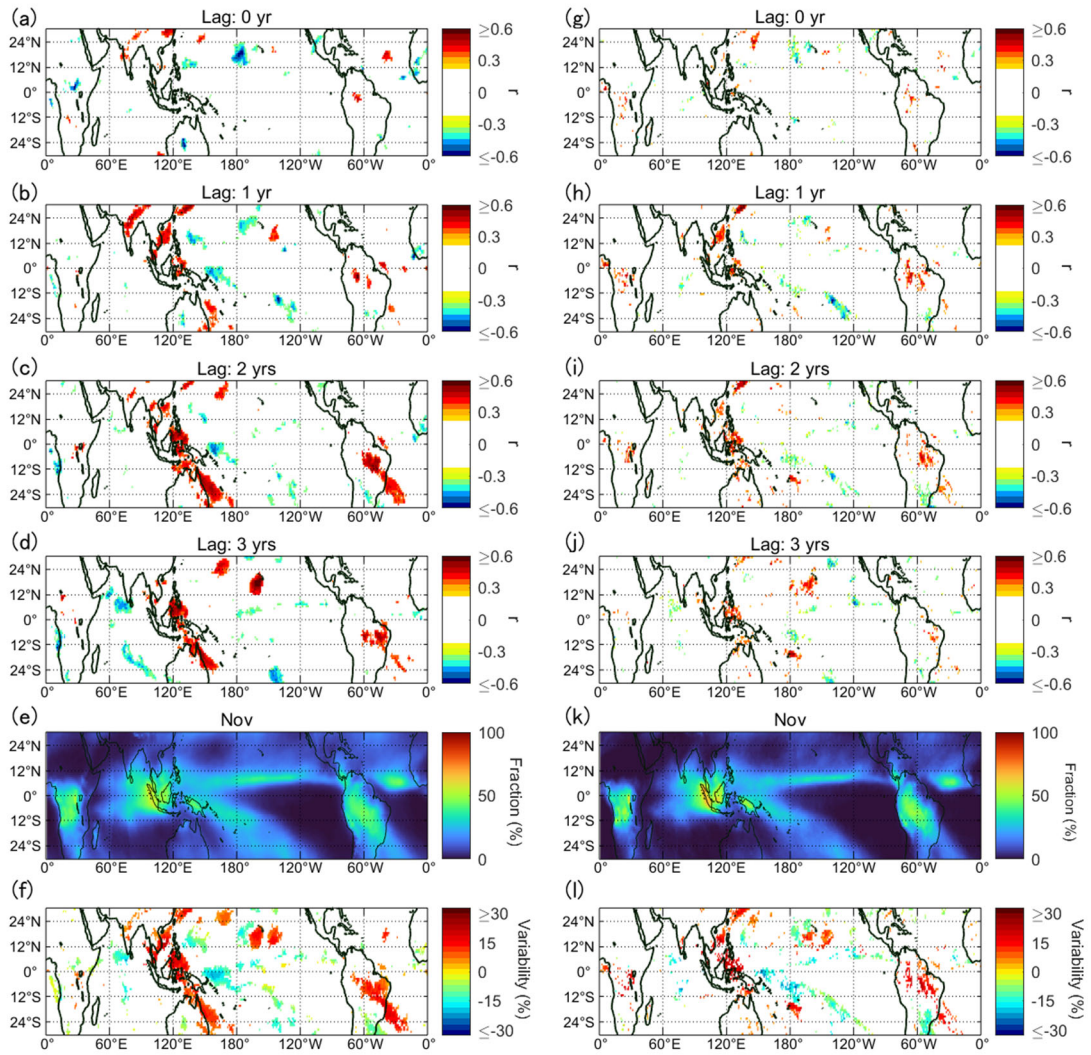


Figure S11. Same as Fig. S1 but for November.

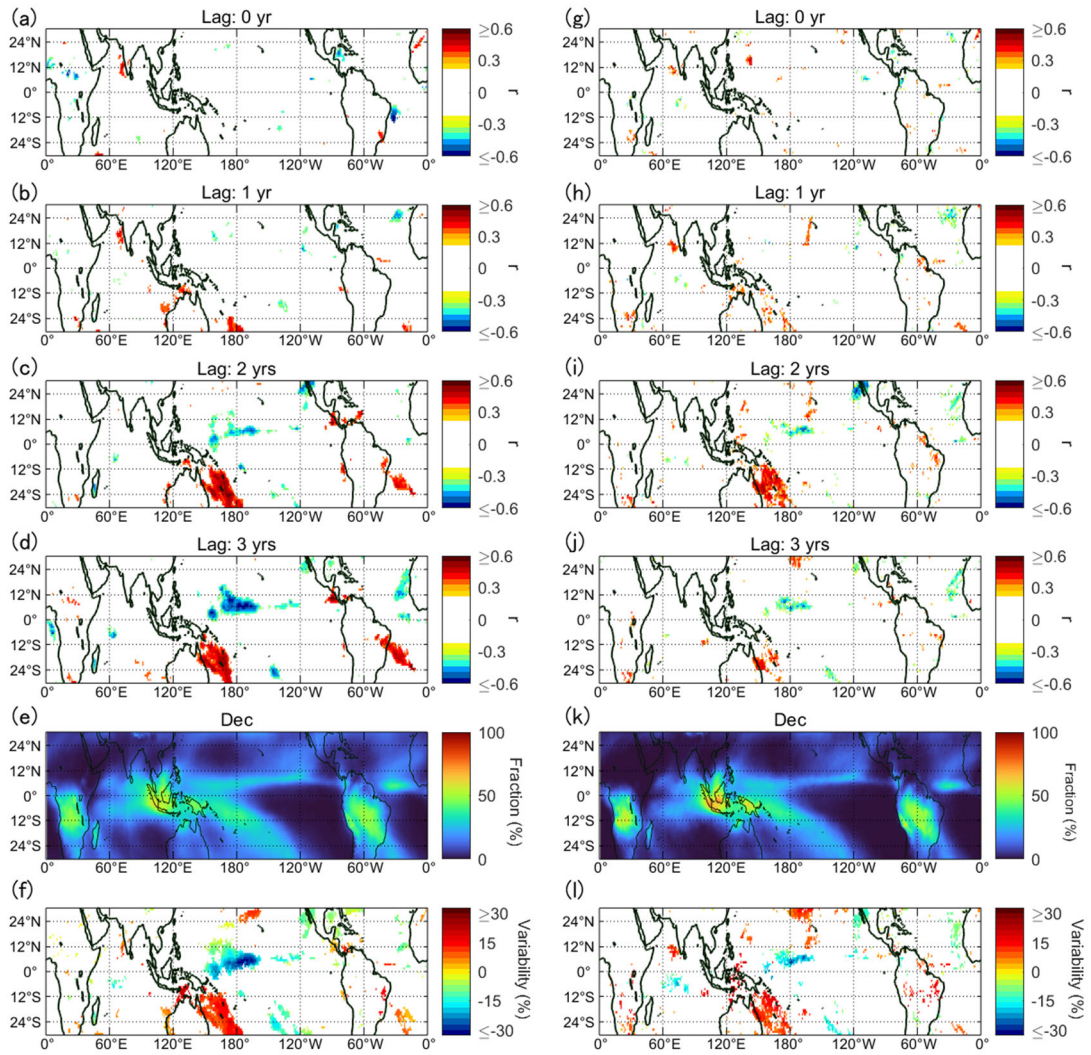


Figure S12. Same as Fig. S1 but for December.

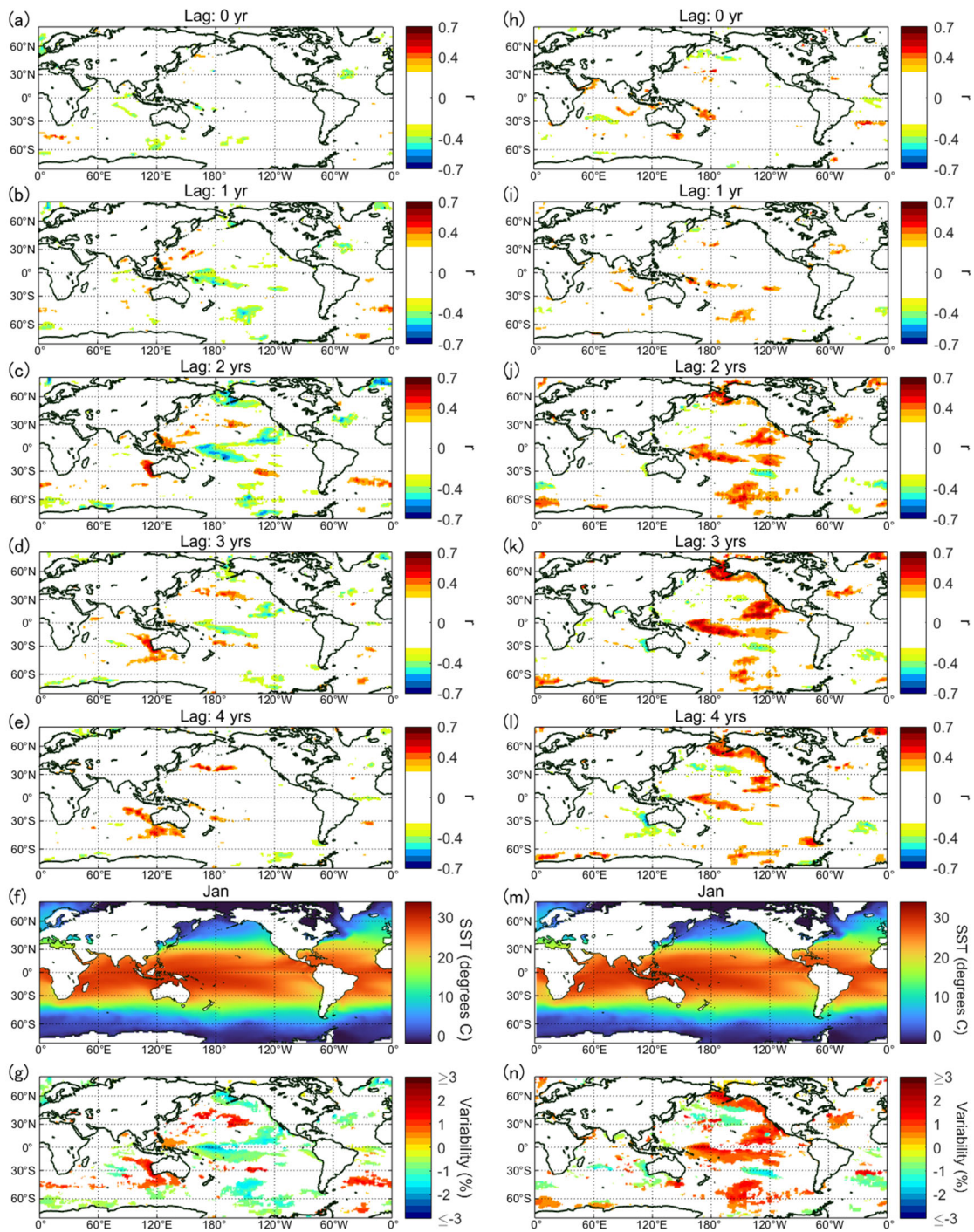


Figure S13. (a-e) Correlation coefficient r ($p \leq 0.05$) between GCR and SST in January for a time lag of 0–4years, respectively. (f) Monthly mean SST. (g) Maximal variability of SST over the GCR cycles. (h-n) Same as (a-g) but for TSI.

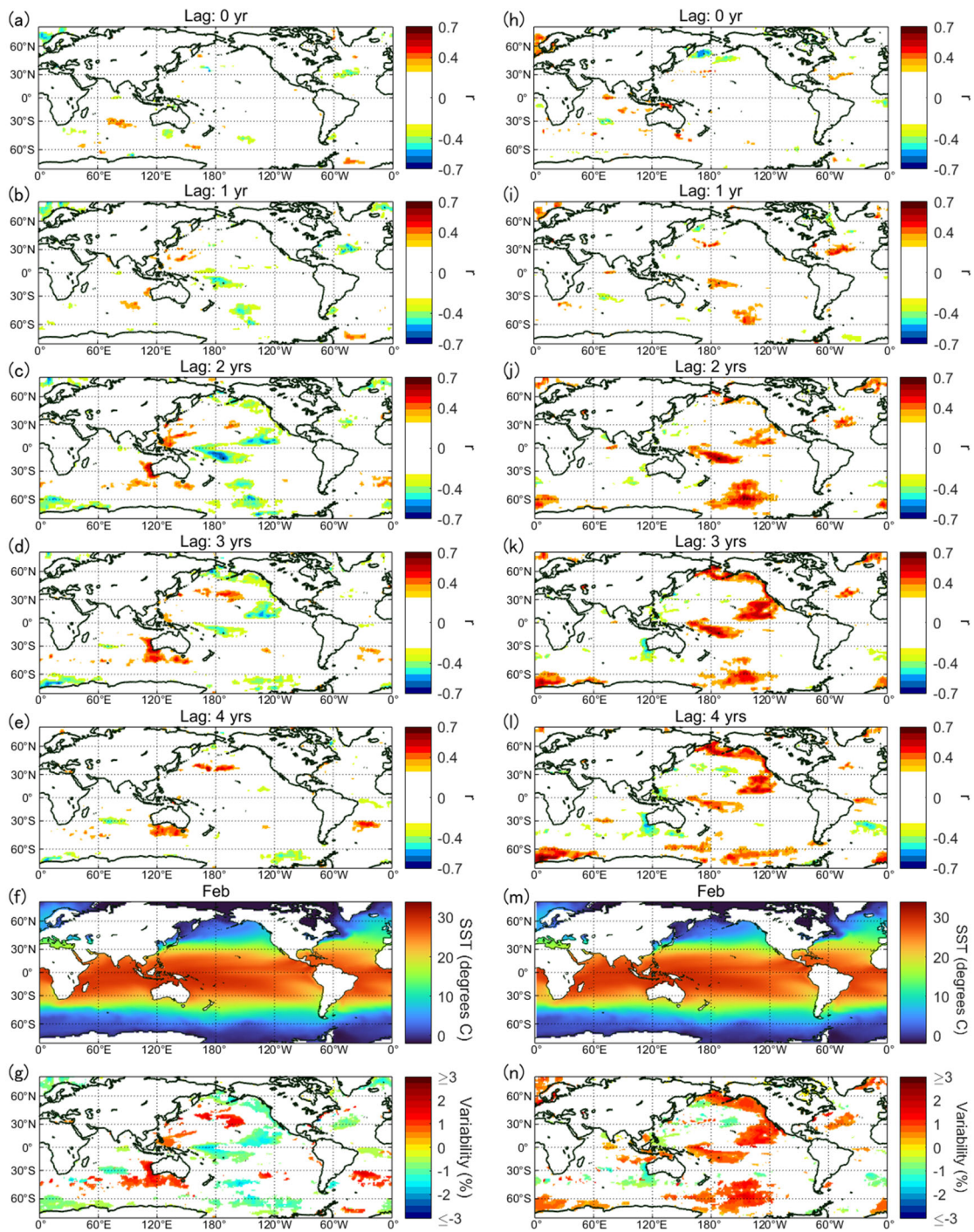


Figure S14. Same as Fig. S13 but for February.

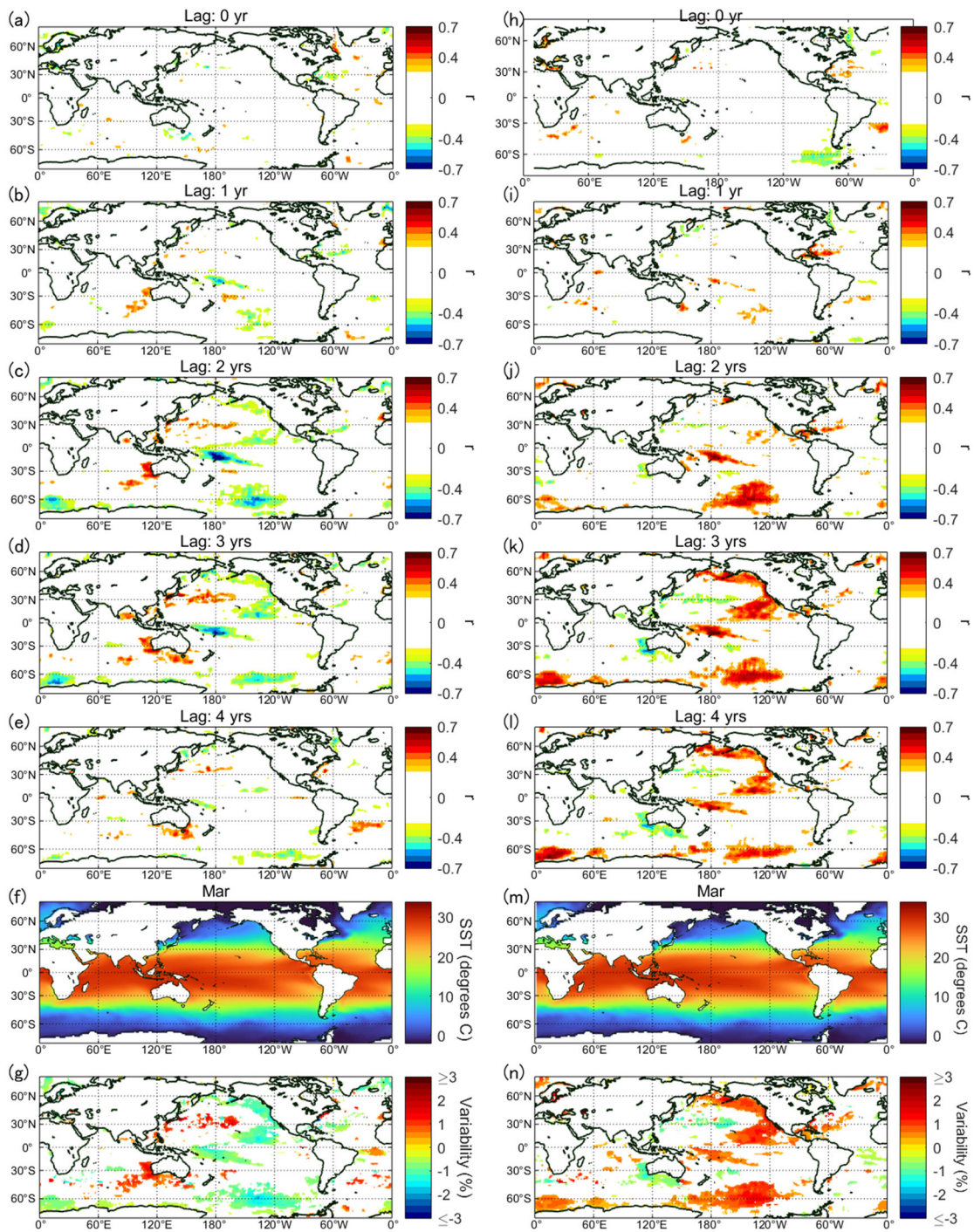


Figure S15. Same as Fig. S13 but for March.

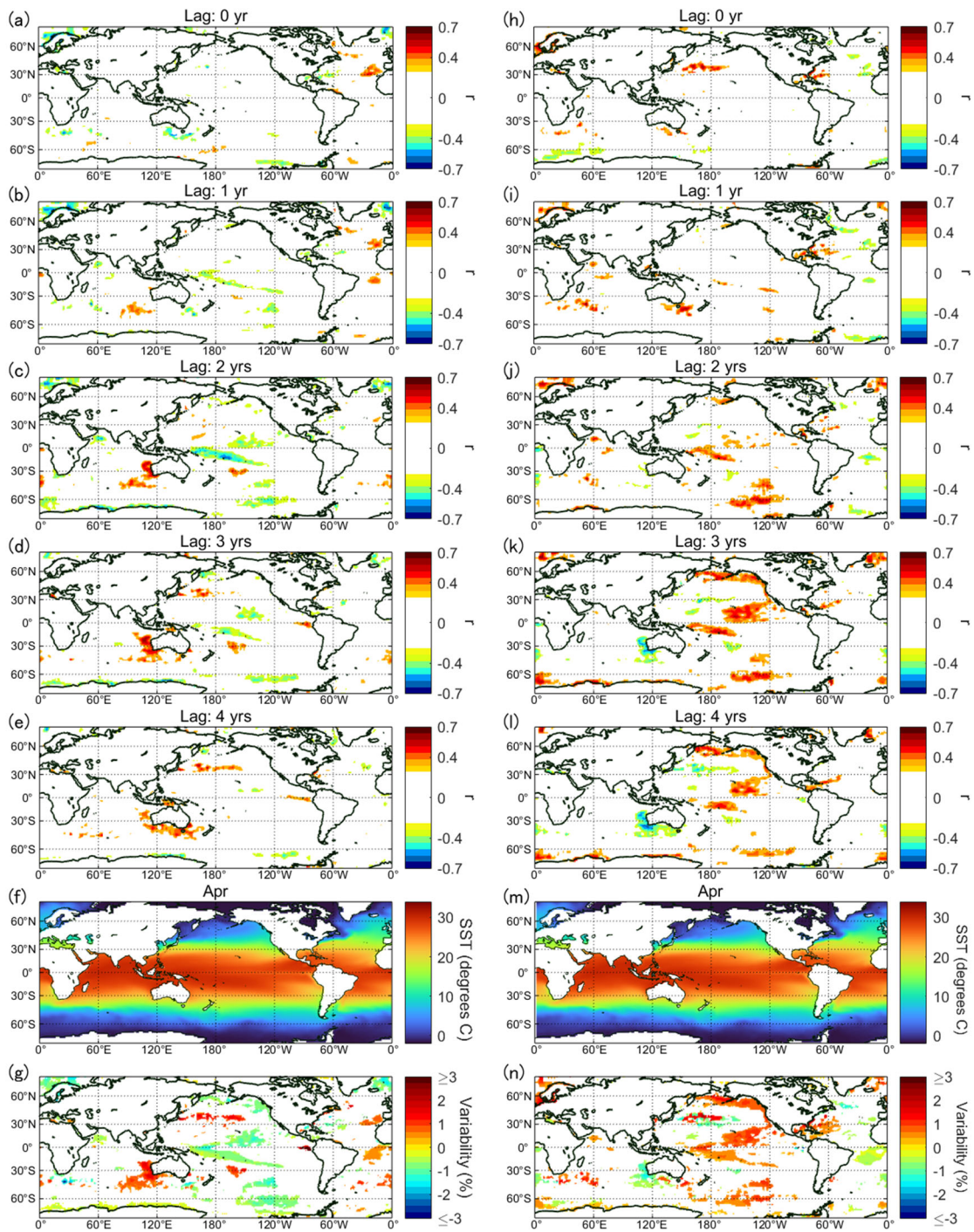


Figure S16. Same as Fig. S13 but for April.

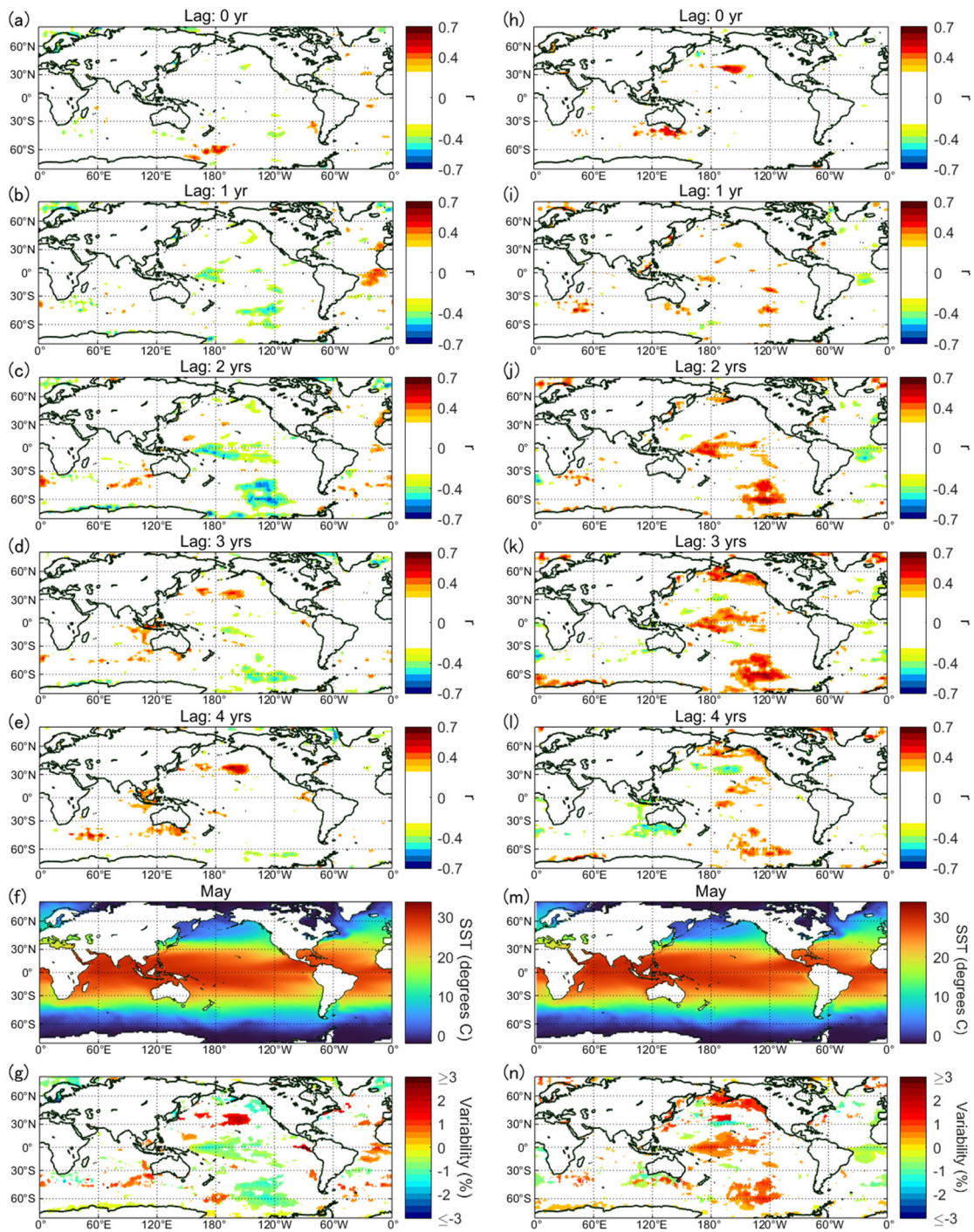


Figure S17. Same as Fig. S13 but for May.

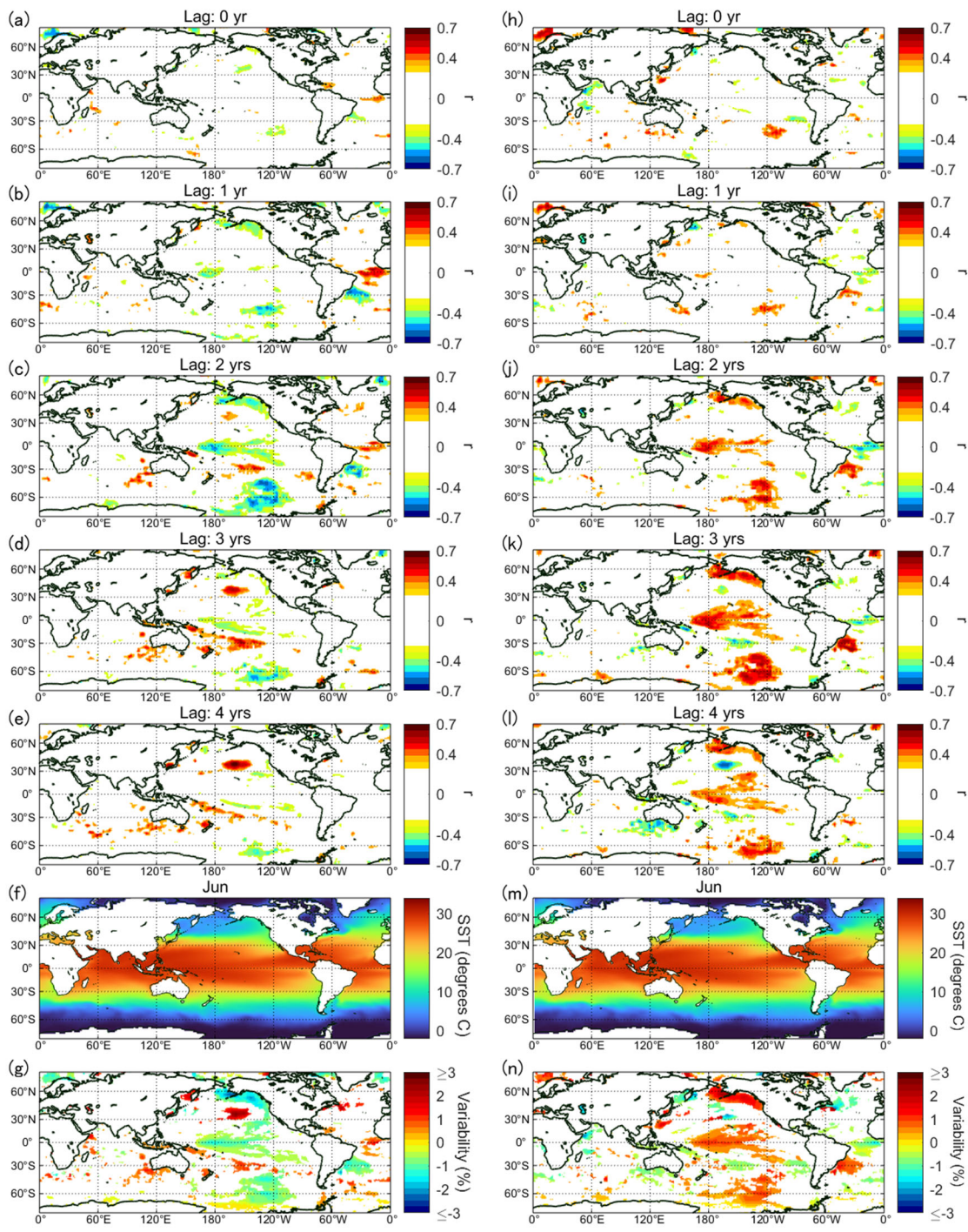


Figure S18. Same as Fig. S13 but for June.

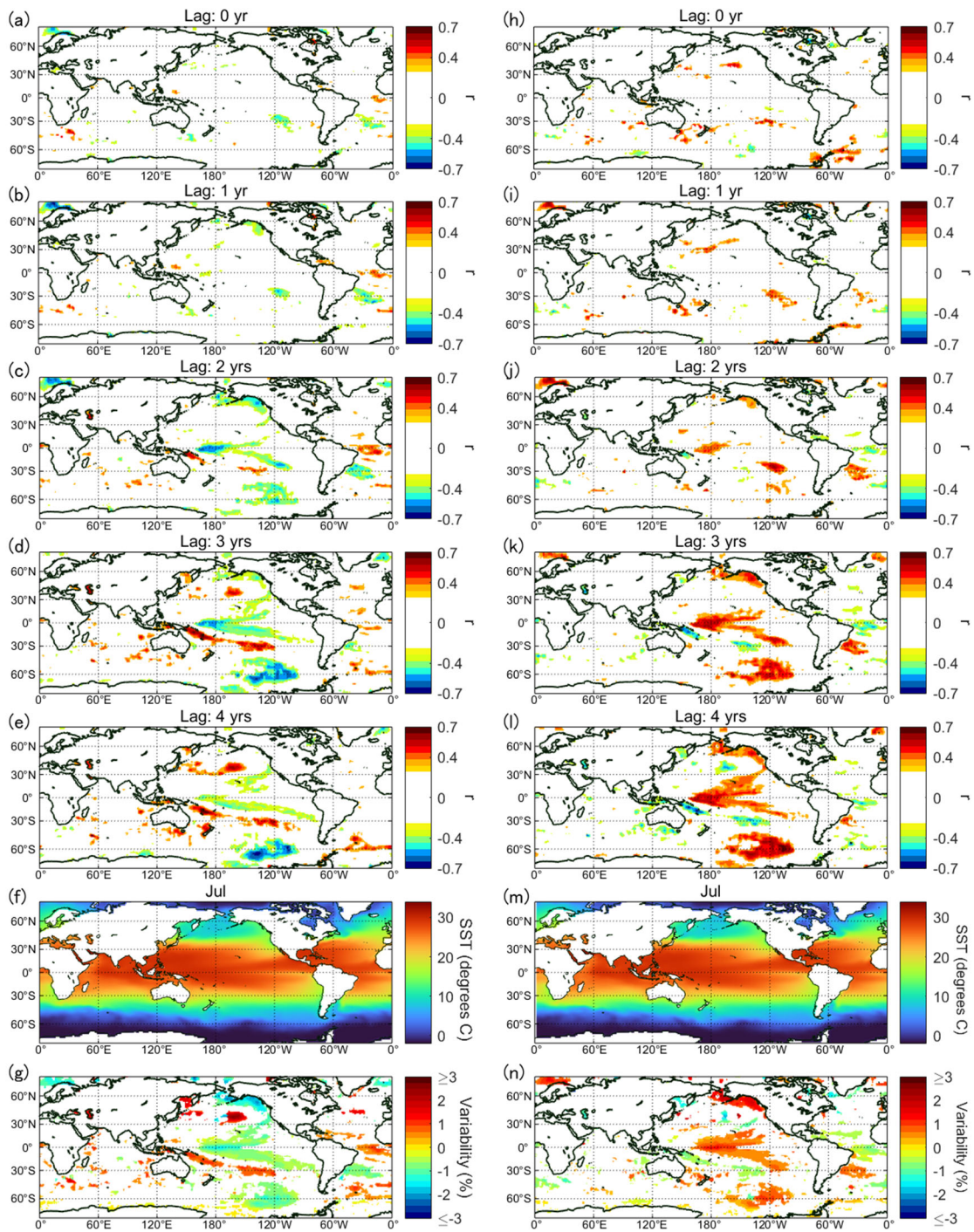


Figure S19. Same as Fig. S13 but for July.

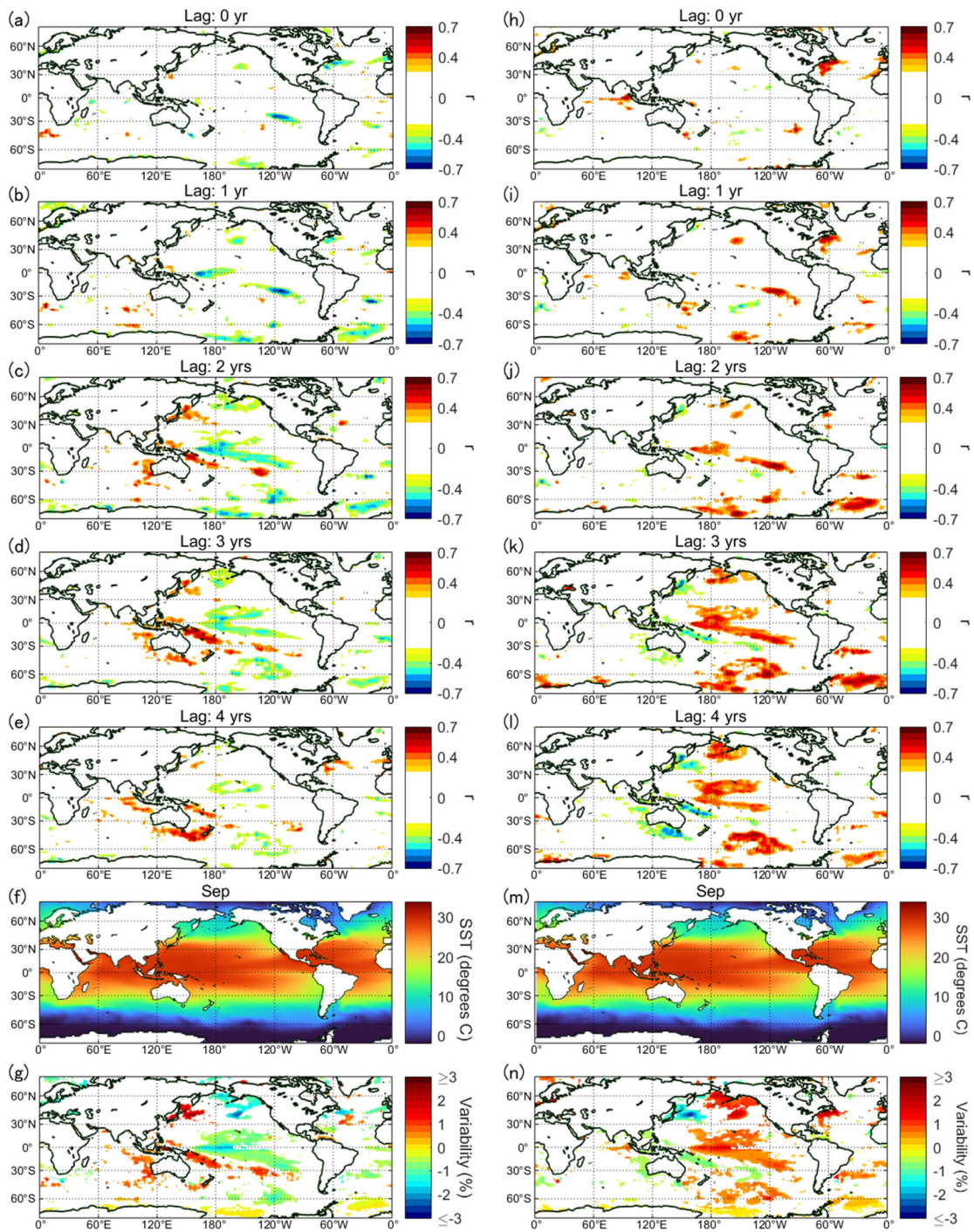


Figure S20. Same as Fig. S13 but for September.

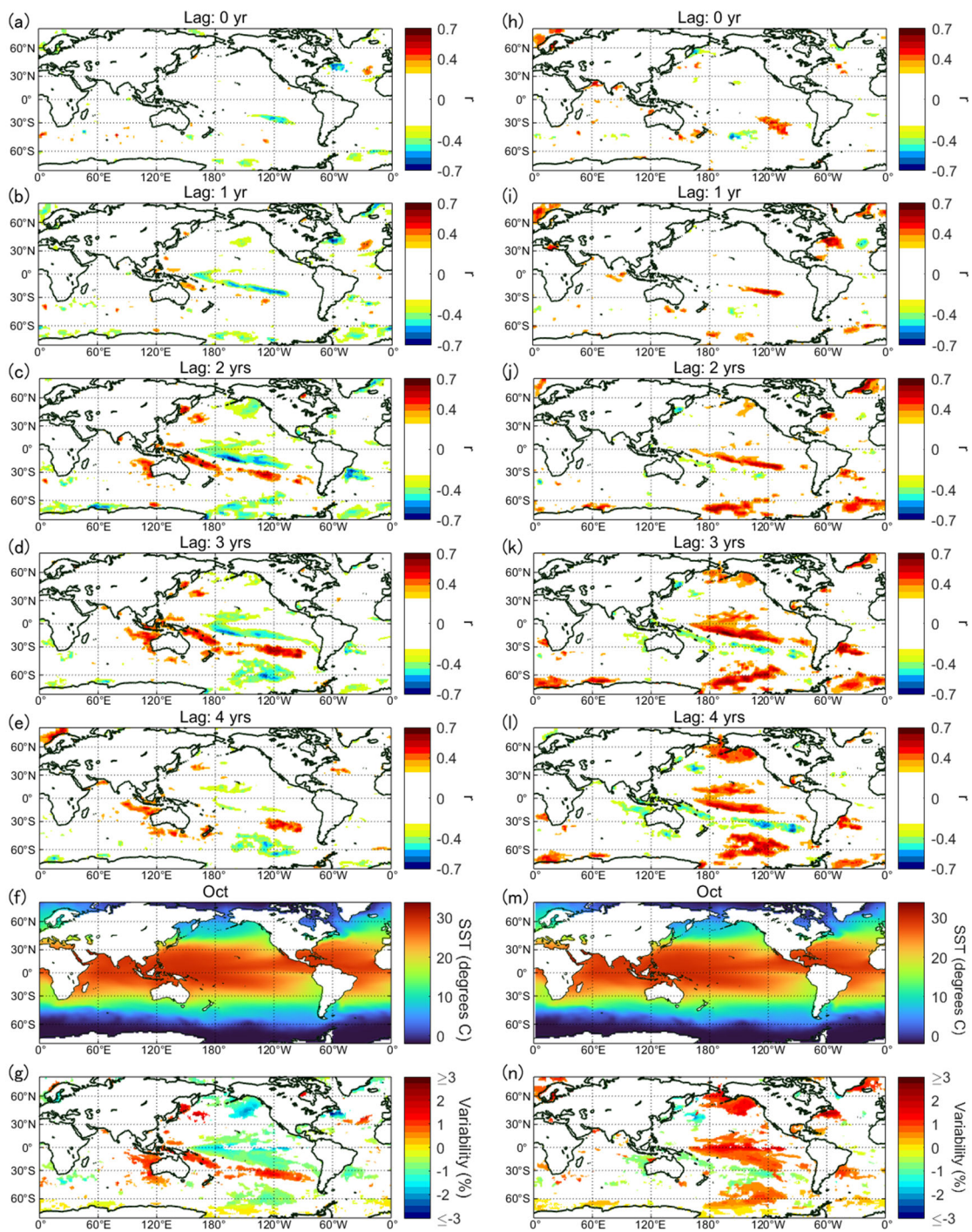


Figure S21. Same as Fig. S13 but for October.

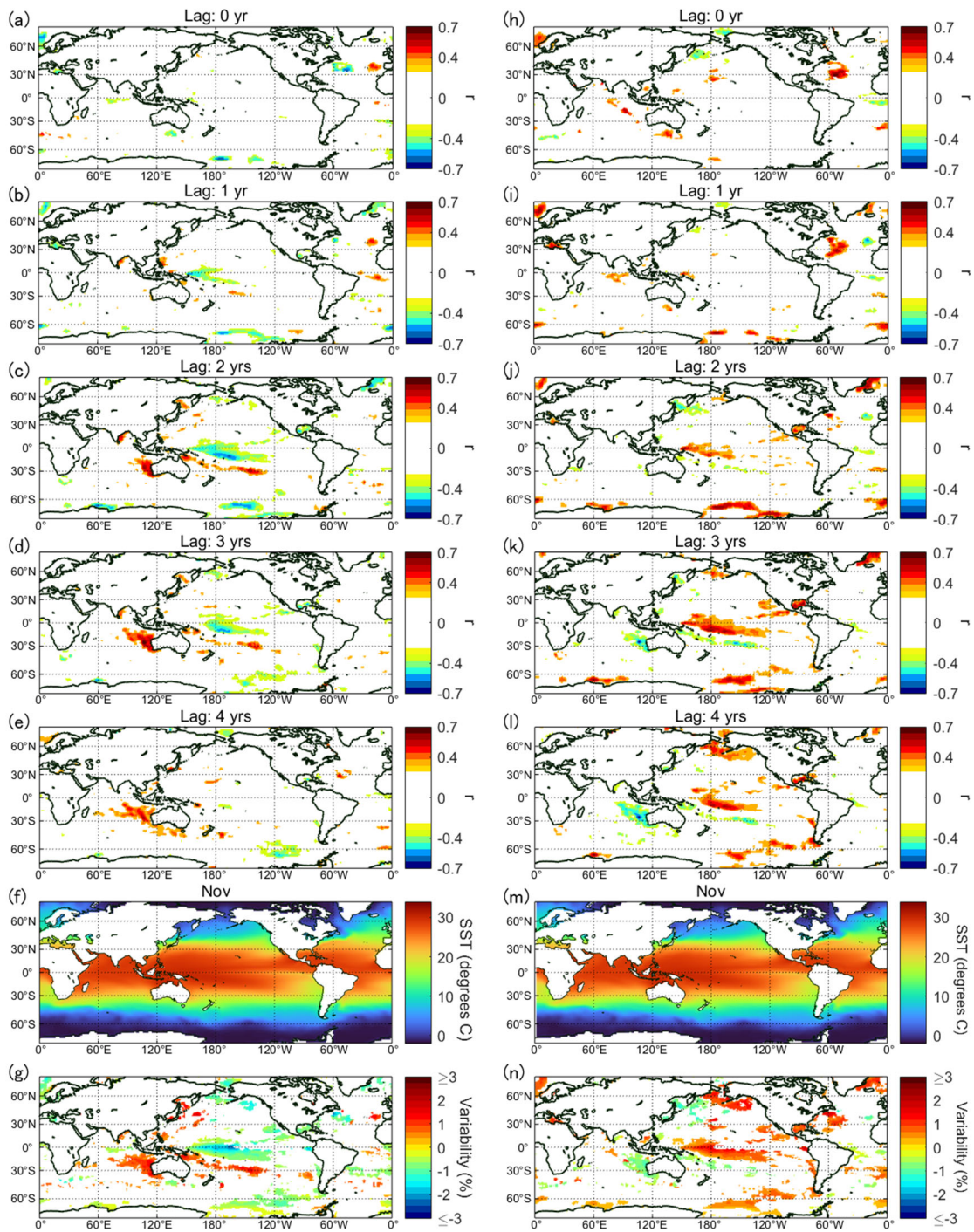


Figure S22. Same as Fig. S13 but for November.

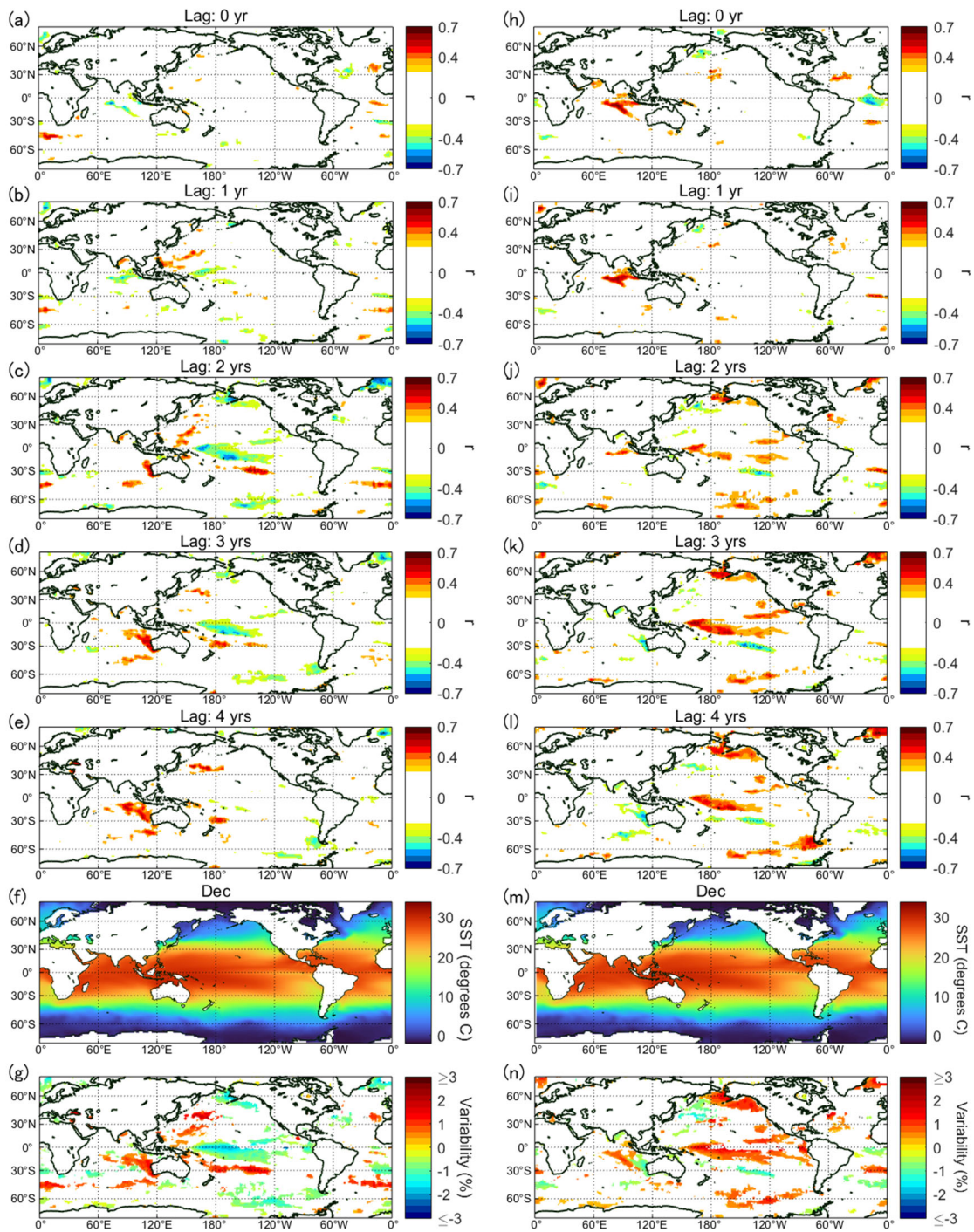


Figure S23. Same as Fig. S13 but for December.

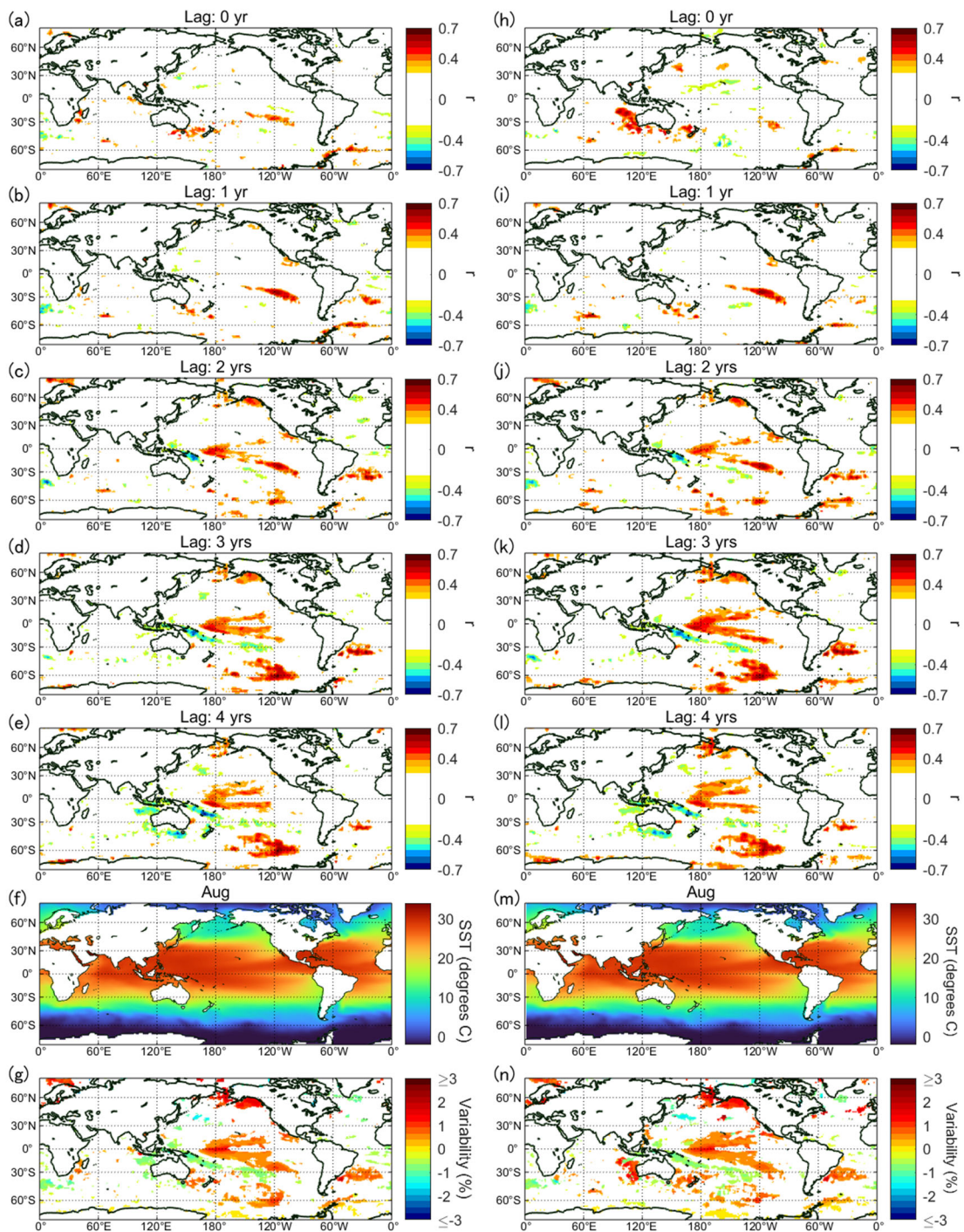


Figure S24. Comparison between SST and SUV/TSI. (a-e) Correlation coefficient r ($p \leq 0.05$) between SUV and SST in August for a lag of 0–4 years, respectively. (f) Monthly mean SST for August. (g) Maximal variability of SST over the SUV cycles. (h-n) Same as (a-g) but for TSI.

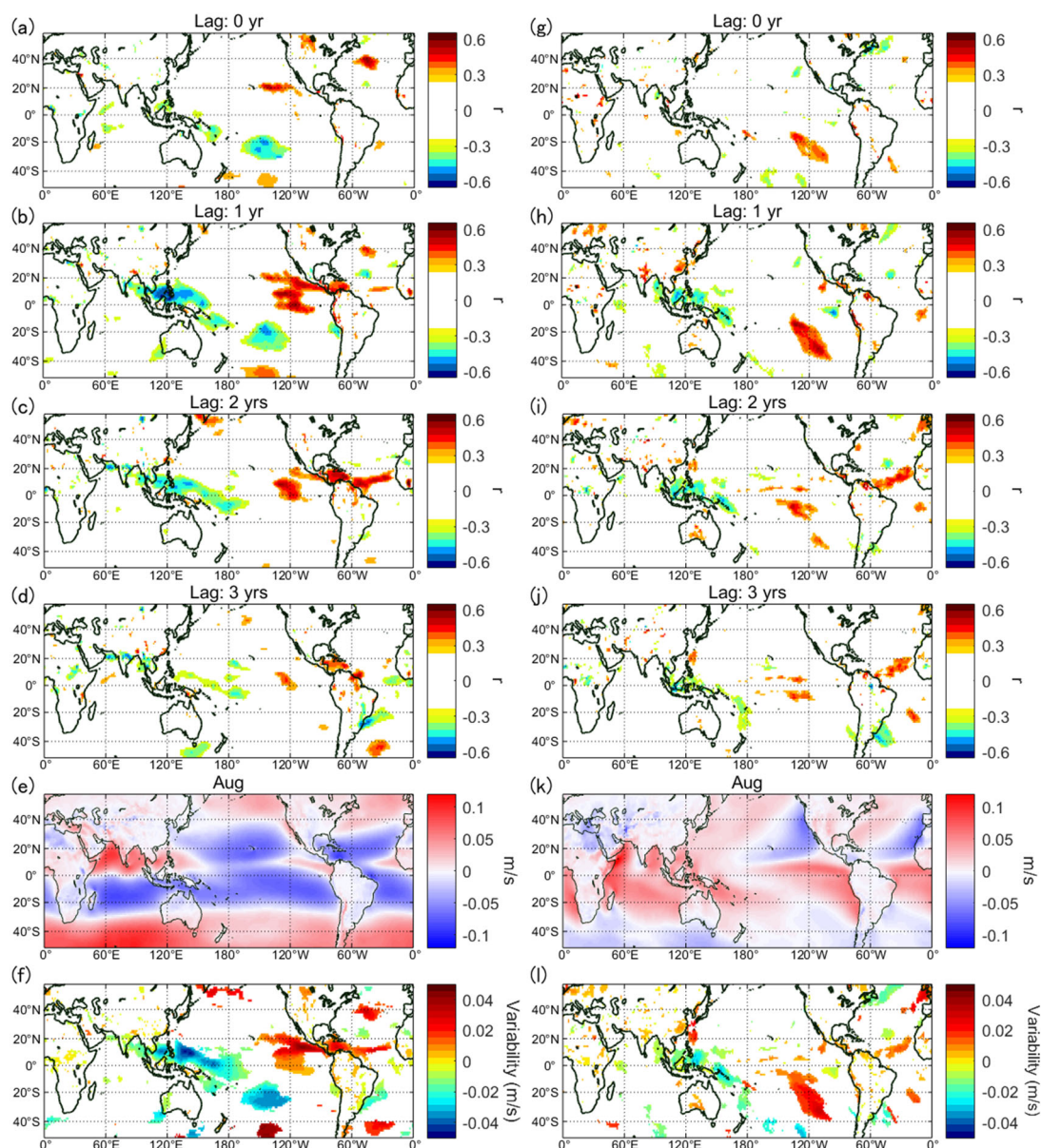


Figure S25. Comparison between the JRA-55 zonal/meridional wind velocity and GCR variation. (a-d) Correlation coefficient r ($p \leq 0.05$) between the zonal wind velocity and GCRs in August for a lag of 0–3 years, respectively. (e) Monthly mean velocity for August. (f) Maximal variability of zonal wind velocity over the GCR cycles. (g-l) Same as (a-f) but for the meridional wind velocity.

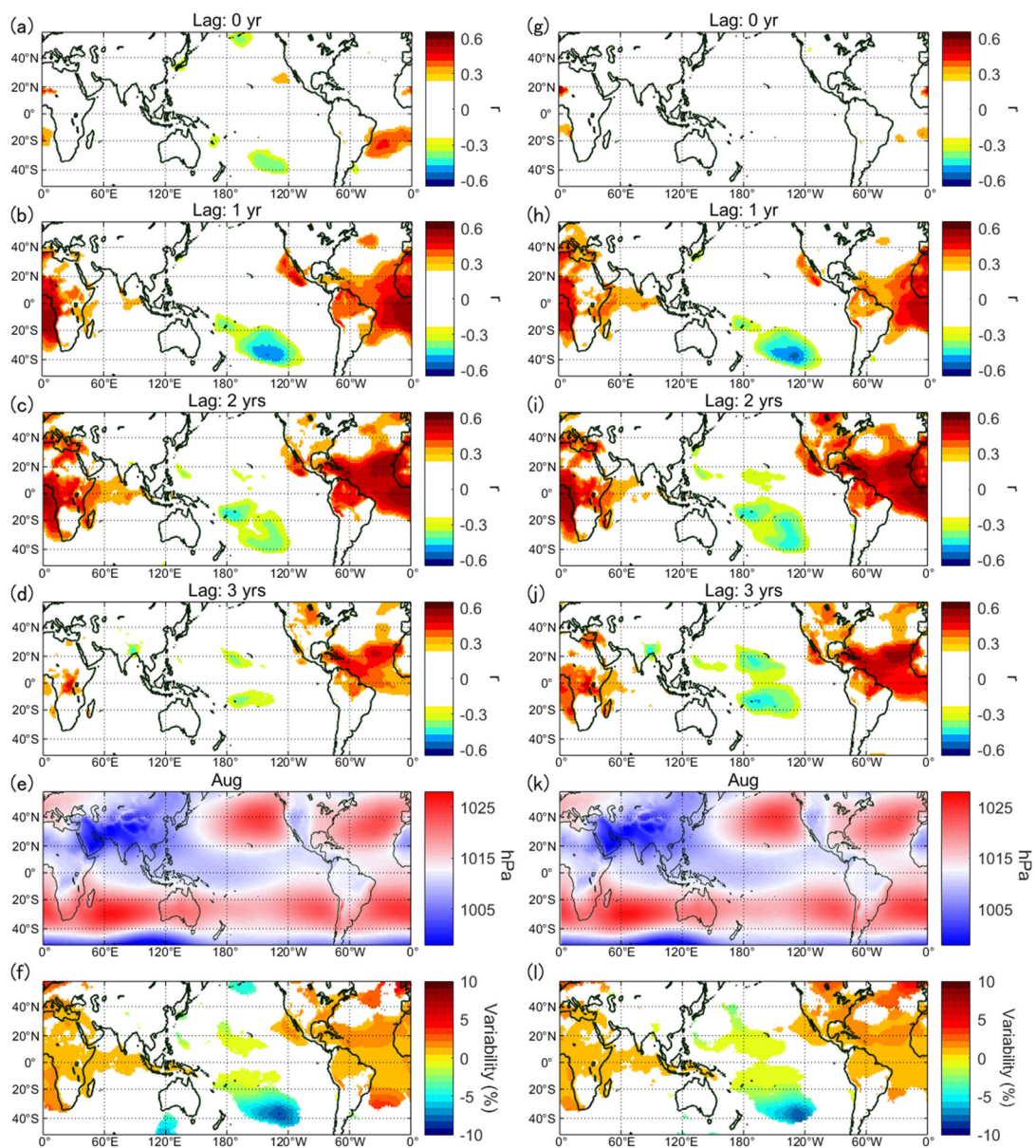


Figure S26. Comparison between the JRA-55 pressure reduced to the mean sea level and the SUV/TSI variations. (a-d) Correlation coefficient r ($p \leq 0.05$) between the pressure and SUV in August for a lag of 0–3 years, respectively. (e) Monthly mean pressure reduced to the mean sea level for August. (f) Maximal variability of pressure over the SUV cycles. (g-l) Same as (a-f) but for TSI.

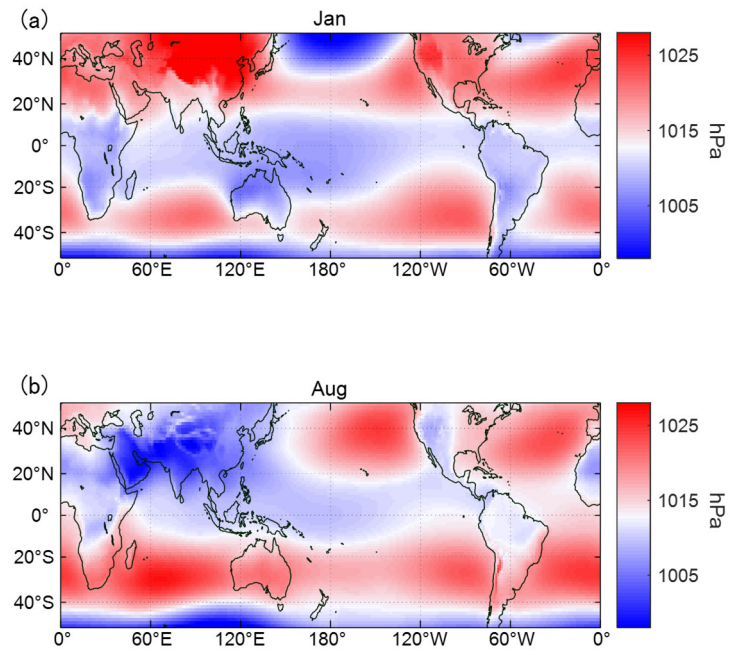


Figure S27. JRA-55 pressure reduced to the mean sea level averaged for 1979–2021 for (a) January and (b) August.

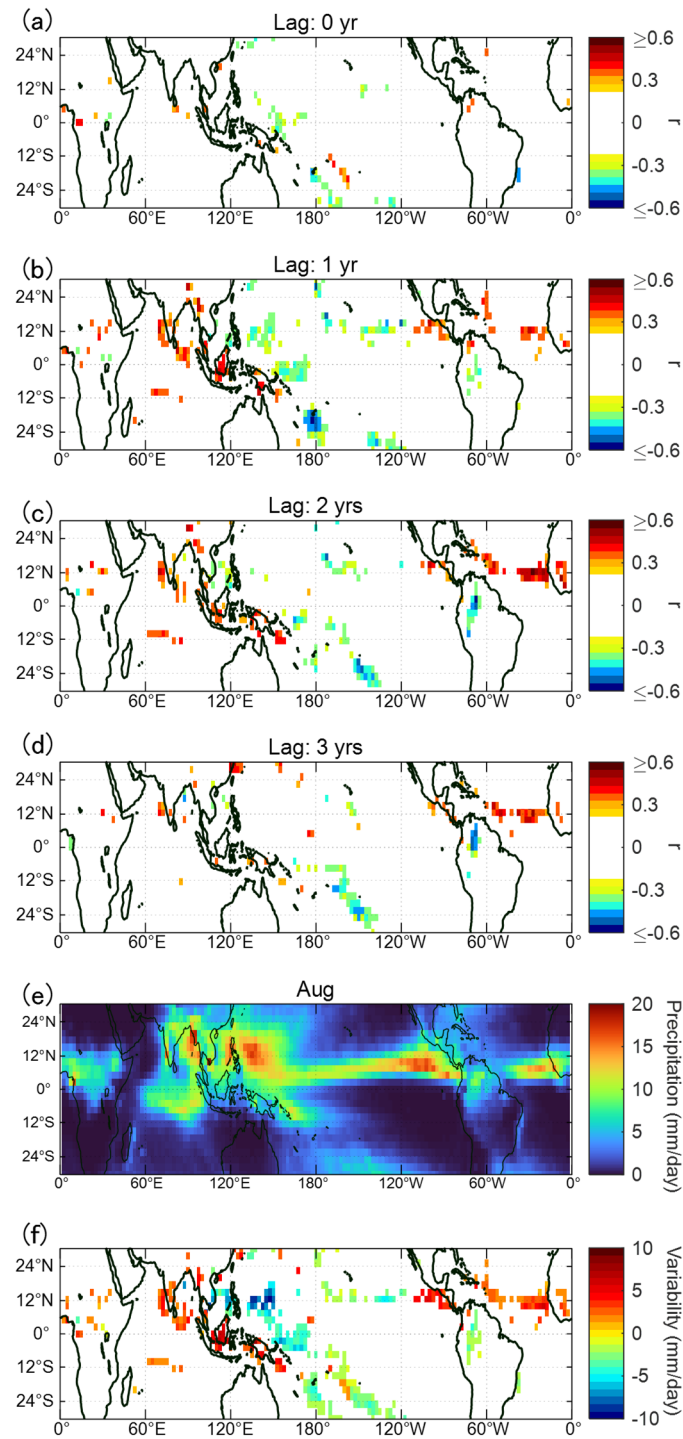


Figure S28. Comparison between the CMAP precipitation data and GCR variation. (a-d) Correlation coefficient r ($p \leq 0.05$) between the precipitation and GCRs in August for a lag of 0–3 years, respectively. (e) Monthly mean precipitation for August. (f) Maximal variability of precipitation over the GCR cycles.

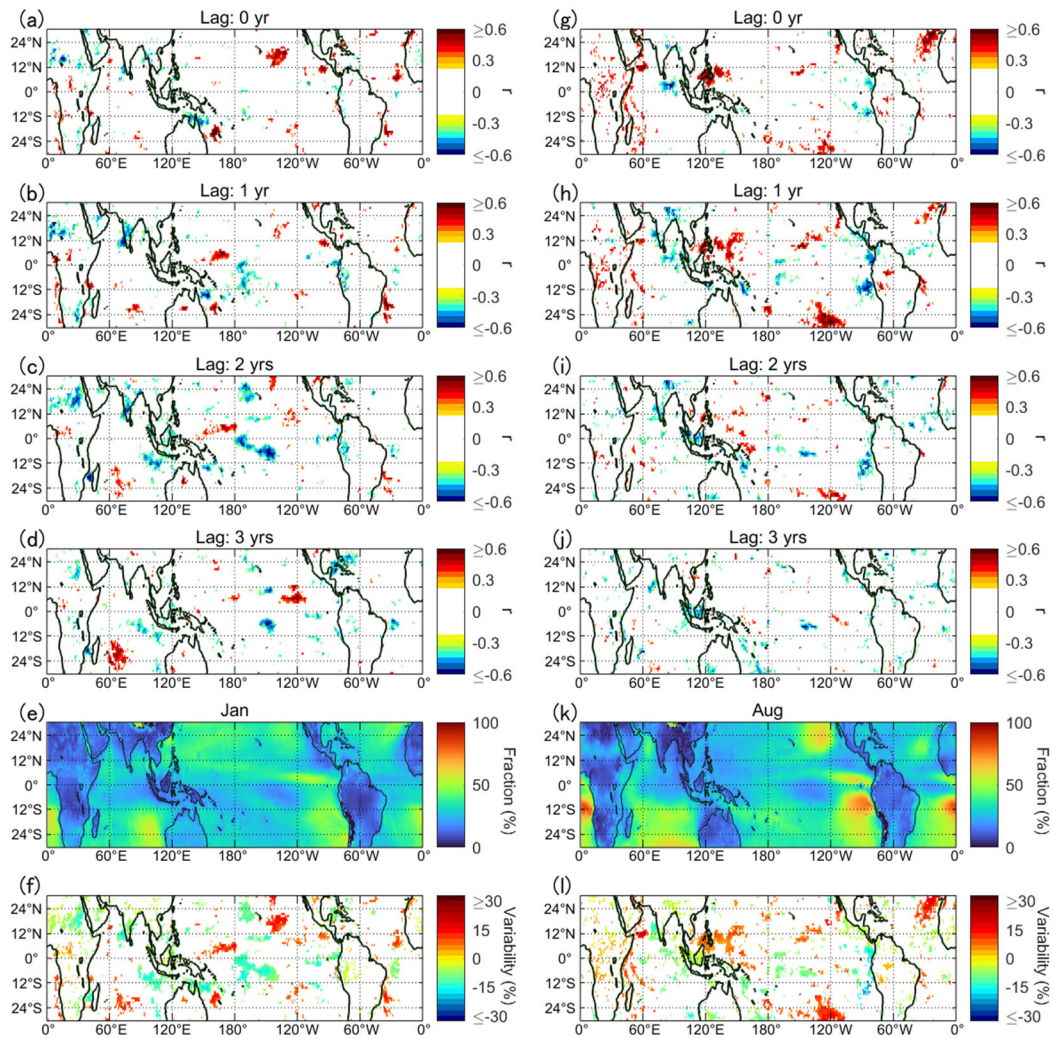


Figure S29. (a-d) Correlation coefficient r ($p \leq 0.05$) between GCRs and the low-altitude cloud fraction in January by ISCCP for a time lag of 0–3 years, respectively. (e) Monthly mean fraction of the low-altitude clouds in January. (f) Maximal variability of the low-altitude cloud fraction over the GCR cycles. (g-l) Same as (a-f) but for August.